Unbalanced emission reductions of different species and sectors in China during COVID-19 lockdown derived by multi-species surface observation assimilation

Lei Kong[1,3], Xiao Tang[*,1,3], Jiang Zhu[2,3], Zifa Wang[1,3,4], Yele Sun[1,3], Pingqing Fu[5], Meng Gao[6], Huangjian Wu[1,3], Miaomiao Lu[7], Qian Wu[1,3], Shuyuan Huang[8], Wenxuan Sui[1], Jie Li[1,3], Xiaole Pan[1,3], Lin Wu[1,3], Hajime Akimoto[9], Gregory R. Carmichael[10]

[1]State Key Laboratory of Atmospheric Boundary Layer Physics and Atmospheric Chemistry (LAPC), Institute of Atmospheric Physics, Chinese Academy of Sciences, Beijing 100029, China
[2]CAS-TWAS Center of Excellence for Climate and Environment Sciences (ICCES), Institute of Atmospheric Physics, Chinese Academy of Sciences, Beijing 100029, China
[3]University of Chinese Academy of Sciences, Beijing 100049, China
[4]Center for Excellence in Regional Atmospheric Environment, Institute of Urban Environment, Chinese Academy of Sciences, Xiamen 361021, China
[5]Institute of Surface-Earth System Science, Tianjin University, Tianjin 300072, China
[6]Department of Geography, State Key Laboratory of Environmental and Biological Analysis, Hong Kong Baptist University, Hong Kong SAR, China
[7]State Environmental Protection Key Laboratory of Urban Ambient Air Particulate Matter Pollution Prevention and Control, College of Environmental Science and Engineering, Nankai University, Tianjin 300350, China
[8]Chengdu University of Information Technology, Chengdu 610225, China
[9]National Institute for Environmental Studies, Onogawa, Tsukuba 305-8506, Japan
[10]Center for Global and Regional Environmental Research, University of Iowa, Iowa City, IA 52242, USA

Correspondence to: Xiao Tang (tangxiao@mail.iap.ac.cn)

Abstract. The unprecedented lockdown of human activities during the COVID-19 pandemic have significantly influenced the social life in China. However, understanding of the impact of this unique event on the emissions of different species is still insufficient, prohibiting the proper assessment of the environmental impacts of COVID-19 restrictions. Here we developed a multi-air pollutant inversion system to simultaneously estimate the emissions of NO_x, SO_2, CO, $PM_{2.5}$ and PM_{10} in China during COVID-19 restrictions with high temporal (daily) and horizontal (15km) resolutions. Subsequently, contributions of emission changes versus meteorology variations during COVID-19 lockdown were separated and quantified. The results demonstrated that the inversion system effectively reproduced the actual emission variations of multi-air pollutants in China during different periods of COVID-19 lockdown, which indicate that the lockdown is largely a nationwide road traffic control measure with NO_x emissions decreased substantially by ~40%. However, emissions of other air pollutants were found only decreased by ~10%, because power generation and heavy industrial processes were not halted during lockdown, and residential activities may actually have increased due to the stay-at-home orders. Consequently, although obvious reductions of $PM_{2.5}$ concentrations occurred over North China Plain (NCP) during lockdown period, the emission change only accounted for 8.6% of $PM_{2.5}$ reductions, and even led to substantial increases of O_3. The meteorological variation instead dominated the changes in $PM_{2.5}$ concentrations over NCP, which contributed 90% of the $PM_{2.5}$ reductions over most parts of NCP region. Meanwhile,

our results suggest that the local stagnant meteorological conditions together with inefficient reductions in $PM_{2.5}$ emissions were the main drivers of the unexpected $PM_{2.5}$ pollution in Beijing during lockdown period. These results highlighted that traffic control as a separate pollution control measure has limited effects on the coordinated control of O_3 and $PM_{2.5}$ concentrations under current complex air pollution conditions in China. More comprehensive and balanced regulations for multiple precursors from different sectors are required to address O_3 and $PM_{2.5}$ pollution in China.

1 Introduction

A novel coronavirus disease (COVID-19) broke out in Wuhan at the end of 2019 but quickly spread across the whole China within a month. To curb the spread of the virus, strict epidemic control measures were implemented by Chinese governments to prevent large gatherings, including strict travel restriction, shutting down of non-essential industries, extended holidays, closing of schools and entertainment houses (Cheng et al., 2020). These restrictions have had a significant impact on the industrial activities and social life, as exemplified by the drop of China's industrial output by 15-30% (https://data.stats.gov.cn/, last accessed on 22 Oct, 2022) and the dramatic decrease of traffic flow by 60–90% in major cities of China during COVID-19 epidemic (http://jiaotong.baidu.com/, last accessed on 22 Oct, 2022), which provides us a natural experiment to examine the responses of the emissions and air quality on the changes in human activities.

It has been well documented that the short-term stringent emission control targeted on power generator or heavy industry enacted by Chinese government during certain societal events, such as the 2008 Olympics Games, 2014 Asia-Pacific Economic Cooperation conference and 2015 China Victory Day Parade, is an effective way to reduce emissions and improve air quality (Okuda et al., 2011; Wang et al., 2014; Tang et al., 2015; Zhang et al., 2016; Wu et al., 2020; Chu et al., 2018). However, different from those stringent emission controls, the COVID-19 restrictions are inclined to affect emissions from sectors more closely to social life whose influence on emissions has still not well been assessed. Previous studies suggest that the COVID-19 restrictions have substantially reduced the China's anthropogenic emissions from almost all sectors (Zheng et al., 2021; Huang et al., 2021; Xing et al., 2020). For example, by using a bottom-up method based on near-real-time activity data, Zheng et al. (2021) reported that the emissions of NO_x, SO_2, CO and primary $PM_{2.5}$ decreased by 36%, 27%, 28% and 24% during COVID-19 restrictions, mostly due to the reductions in industry and transportation sector. Xing et al. (2020), by using a response model, estimated stronger COVID-19 shutdown effects on emissions over the North China Plain (NCP) with emissions of NO_x, SO_2 and primary $PM_{2.5}$ dropped by 51%, 28% and 63%, respectively. Others argue that the COVID-19 restriction may mainly affect the emissions from transportation, light industry and manufacturing, while it has much smaller effects on the emissions from the power generator and heavy industry because of their non-interruptible processes (Chu et al., 2021; Hammer et al., 2021; Le et al., 2020; Zhao et al., 2020). Moreover, the residential emissions may even increase during the COVID-19 lockdown due to the increased demanding for space heating and cooking with the stay-at-home orders. Therefore, Le et al. (2020) only considered the NO_x reductions during COVID-19 restrictions in their investigation of the severe haze during COVID-19 lockdown, and similarly, Hammer et al. (2021) only considered the emission reductions in the

69 transportation sector. This indicates that there has large uncertainty in the current understanding of the effects of COVID-19

70 restrictions on the emissions of different species.

71   Quantification of the emission changes of different species and different sectors during the COVID-19 lockdown is thus

72 necessary for the comprehensive understanding of the environmental impacts of COVID-19 restrictions. In particular, although

73 observations indeed show decreases of air pollutant concentrations during COVID-19 restrictions (Fan et al., 2020; Wang et

74 al., 2021; He et al., 2020; Shi and Brasseur, 2020), the air quality improvement is much smaller than the expected (Shi et al.,

75 2021; Diamond and Wood, 2020; Yan et al., 2022). Moreover, severe haze still occurred in northern China (Sulaymon et al.,

76 2021; Le et al., 2020) and O_3 concentrations even showed significant increases (Zhang et al., 2021; Li et al., 2020). A number

77 of studies were conducted to explain this anomalistic air quality change by analyzing the effects of emission changes,

78 meteorological variations and secondary production (Huang et al., 2021; Le et al., 2020; Hammer et al., 2021; Zhao et al.,

79 2020; Zhao et al., 2021; Sulaymon et al., 2021; Wang et al., 2020; Li et al., 2021). However, due to the unknown emission

80 changes during COVID-19 restrictions, the emission reduction scenarios that used to represent the COVID-19 shutdown effects

81 varied among different studies and did not consider the spatial and temporal heterogeneity of the emission changes, leading to

82 biases in the model simulation (Zhao et al., 2021; Li et al., 2021; Hammer et al., 2021; Zheng et al., 2021) and uncertainty in

83 the quantification of the contributions of different factors.

84   Pioneer studies by Zheng et al. (2021) and Forster et al. (2020) have derived multi-air pollutant emissions from social

85 activity data using a bottom-up method, but due to the lack of detailed social activity data, large uncertainties existed in their

86 estimates. The meteorologically and seasonally driven variability of the concentrations of air pollutants also prohibit drawing

87 fully quantitative conclusions on the changes of emissions based on observations alone (Levelt et al., 2022). The emission

88 inversion technique, which takes advantage of the chemical transport model (CTM) and real-time observations, provides an

89 attractive way to estimate the sector-specific and space-based emission changes during COVID-19 restrictions, as shown in

90 Zhang et al. (2020), Zhang et al. (2021), Feng et al. (2020) and Hu et al. (2022). However, these studies only inversed the

91 emissions of single species (e.g., NO_x and SO_2) without insights into multiple species. In view of this discrepancy, in this study

92 we developed a multi-air pollutant inversion system to simultaneously estimated the multi-air pollutant emissions in China,

93 including NO_x, SO_2, CO, $PM_{2.5}$ and PM_{10}, during the COVID-19 restrictions using an ensemble Kalman filter (EnKF) and

94 surface observations from the China National Environmental Monitoring Centre (CNEMC). Subsequently, the inversed

95 emission inventory was used to quantify the contributions of emission changes versus meteorology variations to the changes

96 in $PM_{2.5}$ and O_3 concentrations over the NCP region during the COVID-19 restrictions.

97 **2 Method and data**

98   We developed a high-resolution multi-air pollutant inversion system to estimate the daily emissions of NO_x, SO_2, CO,

99 $PM_{2.5}$ and PM_{10} in China from 1 Jan to 29 Feb 2020 when the COVID-19 pandemic was at its most serious and the effects of

100 the COVID-19 restrictions were most profound in China. This system uses the NAQPMS (Nested Air Quality Prediction

101 Modelling System) model as the forecast model and the EnKF coupled with the state argumentation method as the inversion
102 method. It has the capabilities of simultaneous inversion of multi-air pollutant emissions at high temporal (daily) and spatial
103 (15km) resolutions. An iteration inversion scheme was also developed in this study to address the large biases in the a priori
104 emissions. In order to better characterize the emission changes during the COVID-19 restrictions, the whole time period was
105 divided into three periods according to different control phases of COVID-19 and the timing of the Chinese Lunar New Year:
106 before lockdown (P1, January 1-20), lockdown (P2, January 21-February 9) and after back-to-work day (P3, February 10-29).
107 Emission changes in different regions of China were also analyzed, including the North China Plain (NCP), Northeast China
108 (NE), Southeast China (SE), Southwest China (SW), Northwest China (NW) and Central regions (defined in Fig. 1) to
109 investigate the responses of emissions to the COVID-19 restrictions in different regions. In the following sections, we briefly
110 introduce each component of the inversion system.

2.1 Chemical transport model and its configuration

112 The NAQPMS model was used as the forecast model to represent the atmospheric chemistry in this study, which has been
113 used in previous inversion studies (Tang et al., 2011; Tang et al., 2013; Kong et al., 2019; Wu et al., 2020), where detailed
114 descriptions of NAQPMS are available. The Weather Research and Forecasting Model (WRF)(Skamarock, 2008) is used to
115 provide the meteorological inputs to the NAQPMS model.

116 Figure 1 shows the modelling domain of this study with a high horizontal resolution of 15 km. The a priori emission
117 inventory used in this study includes monthly anthropogenic emissions from the HTAP_v2.2 emission inventory for the base
118 year of 2010 (Janssens-Maenhout et al., 2015), biomass burning emissions from the Global Fire Emissions Data base (GFED)
119 version 4 (Randerson et al., 2017; Van Der Werf et al., 2010), biogenic volatile organic compound (BVOC) emissions from
120 MEGAN-MACC (Sindelarova et al., 2014), marine volatile organic compound emissions from the POET database (Granier et
121 al., 2005), soil NO_x emissions from the Regional Emission inventory in Asia (Yan et al., 2003) and lightning NO_x emissions
122 from Price et al. (1997). Chemical top and boundary conditions were provided by the global CTM MOZART (Model for
123 Ozone and Related Chemical Tracers) (Brasseur et al., 1998; Hauglustaine et al., 1998). We assumed no monthly variations in
124 the a priori emission inventory and used January's emission inventory for the whole simulation period so that the emission
125 variation was solely derived from the surface observations. A two-week free run of NAQPMS was conducted as a spin-up
126 time. For each day's meteorological simulation, a 36-h free run of WRF was conducted, of which the first 12-h simulation was
127 a spin-up run and the next 24-h simulation provided the meteorological inputs to NAQPMS. Initial and boundary conditions
128 for the meteorological simulation were provided by the National Center for Atmospheric Research/National Center for
129 Environment Prediction (NCAR/NCEP) 1° ×1° reanalysis data. Evaluation results for the WRF simulation are available in
130 Text S1 in Supplement.

2.2 Surface Observations

The hourly concentrations of NO_2, SO_2, CO, $PM_{2.5}$ and PM_{10} from CNEMC were used in this study to estimate the emissions during COVID-19. The spatial distributions of these observation sites are shown in Fig. 1, which contains 1436 observation sites covering most regions of China. Before assimilation, outliers of observations were first filtered out using the automatic outlier detection method developed by Wu et al. (2018) to prevent the adverse effects of the outliers on data assimilation. Then, the hourly concentrations were averaged to the daily values for the inversions of daily emissions.

The observation error is one of the key inputs to the data assimilation, which together with the background error determine the relative weights of the observation and background values on the analysis. The observation error includes measurement error and representativeness error. The measurement error of each species was designated according to the officially released documents of the Chinese Ministry of Ecology and Environmental Protection (HJ 193-2013 and HJ 654-2013, available at http://www.cnemc.cn/jcgf/dqhj/, last accessed on 22 Oct 2022), which is 5% for $PM_{2.5}$ and PM_{10} and 2% for SO_2, NO_2 and CO. A representativeness error arises from the different spatial scales that the discrete observation data and model simulation represent, which was estimated based on the previous study by Li et al. (2019) and Kong et al. (2021). It should be noted that the NO_2 measurement from CNEMC is made by the chemiluminescent analyser with a molybdenum converter. Due to the interference of HNO_3, PAN and alkyl nitrates (AN), the NO_2 concentrations can be overestimated (Dunlea et al., 2007; Lamsal et al., 2008) that may lead to spurious decreases in NO_x emissions during the lockdown period. Previous studies usually use chemical transport model to simulate NO_x, HNO_3, PAN and AN to produce correction factors (CFs) for the NO_2 measurements (Cooper et al., 2020; He et al., 2022) using the following relationship proposed by Lamsal et al. (2008):

$$CF = \frac{[NO_2]}{[NO_2]+0.95[PAN]+0.35[HNO_3]+\sum[AN]} \qquad (1)$$

but the calculation of CF could be affected by the simulation errors in the model caused by uncertainties in emission inventory or other error sources, which may contaminate the observations. Therefore, similar to Feng et al. (2020), we did not correct the NO_2 measurement in our inversion of NO_x emissions since there were large uncertainties in the NO_x emissions during the COVID-19 pandemic that possibly led to erroneous CF. Since the EnKF considered the errors in observations through the use of observation error covariance matrix, the chemiluminescence monitor interference to NO_2 measurement were treated as the observation error during the assimilation. A sensitivity inversion experiment was also conducted based on the corrected NO_2 measurement using CF, which suggests that the chemiluminescence monitor interference only have small impacts on the inversed NO_x emission in terms of magnitude and its variation during COVID-19 pandemic. Detailed results of the sensitivity experiment are available in Text S2 in Supplement.

2.3 Inversion estimation scheme

The EnKF coupled with the state augmentation method was used in this study to constrain the emissions of multiple species. EnKF is an advanced data assimilation method proposed by Evensen (1994) that features representation of the uncertainties of the model state by a stochastic ensemble of model realizations. Different from the mass balance method used

in Zhang et al. (2020) and Zhang et al. (2021) that has difficulties in accounting for nonlinear relationship between emissions and concentrations and is more suitable for short-lived species (e.g. NO_x) under relatively coarse (>1°) resolutions (Streets et al., 2013), the EnKF can consider the indirect relationship between emissions and concentrations caused by complex physical and chemical processes in the atmosphere through the use of flow-dependent background error covariance produced by ensemble CTM forecasts (Evensen, 2009; Miyazaki et al., 2012). Compared with the four-dimensional variational assimilation method used in Hu et al. (2022), the EnKF method has comparable computational cost (Skachko et al., 2014) but is more easily implemented without the need to develop complicated adjoint models for complex CTMs. The state augmentation method is a commonly used parameter estimation method (Tandeo et al., 2020), in which the emissions of multi species are treated as state variable and are simultaneously updated according to the relationship between the emissions and concentrations of related species. Due to the chemical reactions in the atmosphere, the concentrations of different species are interrelated with each other. For example, the ambient $PM_{2.5}$ is not only primarily emitted, but also formed secondarily through reactions with several gaseous precursors, such as NO_2 and SO_2. This means that the estimations of $PM_{2.5}$ emission by single inversed estimation method could be biased if the errors in NO_2 and SO_2 emissions were not corrected synchronously. Therefore, it is beneficial to do the multi-species inversion estimation which can provide more constraints on the atmospheric chemical system and lead to more reasonable inversion results. Meanwhile, the use of EnKF method coupled with the state augmentation method allows the estimations of multi-species emissions almost without additional computational cost.

Appropriate estimation of the uncertainty in emissions and chemical concentrations is important for the performance of inversion estimation using EnKF. Since the source emission data over mainland China in HTAP_v2.2 inventory is obtained from the MIX inventory (Li et al., 2017b) , the uncertainties of emissions of different species, including PMF, PMC, BC, OC, NO_x, CO, SO_2, NH_3 and NMVOC (nonmethane volatile organic compounds), were obtained from Li et al. (2017b) and Streets et al. (2003), which were represented by an ensemble of perturbed emissions generated by multiplying the a priori emissions with a perturbation factor $\beta_{i,s}$:

$$E_{i,s} = \beta_{i,s} \circ E_s^p, \ i = 1,2,\cdots N_{ens} \tag{2}$$

where $E_{i,s}$ represents the vector of the ith member of perturbed emissions for species s, E_s^p represents the a priori emissions for this species, $\circ$ denotes the schur product and N_{ens} denotes the ensemble size. In this way, the adjustment of emissions is equivalent to the adjustment of perturbation factors.

In terms of the uncertainty in chemical concentrations, considering that emission uncertainty is the major contributor to the uncertainties in air quality modelling, especially during the COVID-19 period when emissions changed rapidly, uncertainties in chemical variables were obtained through ensemble simulations driven by perturbed emissions. The ensemble size was chosen as 50 to maintain the balance between the filter performance and computational cost. After the ensemble simulations, emissions of multiple species were updated using a deterministic form of EnKF (DEnKF) proposed by Sakov and Oke (2008), which is formulated by

$$\overline{x^a} = \overline{x^b} + P_e^b H^T \left(H P_e^b H^T + R \right)^{-1} \left(y^o - H\overline{x^b} \right) \tag{3}$$

196 $\quad \overline{x^b} = \frac{1}{N}\sum_{i=1}^{N} x_i^b \,; X_i^b = x_i^b - \overline{x^b}$ (4)

197 $\quad \mathbf{P_e^b} = \frac{1}{N-1}\sum_{i=1}^{N} X_i^b\left(X_i^b\right)^{\mathrm{T}}$ (5)

198 where x denotes the state variables; b the background state (a priori); a the analysis state (posteriori); $\mathbf{P_e^b}$ the ensemble-

199 estimated background error covariance matrix and N the ensemble size. y^o represents the vector of observations with an error

200 covariance matrix of $\mathbf{R}$. $\mathbf{H}$ is the linear observational operator that maps the m-dimensional state vector x to a p- (number of

201 observations) dimensional observational vector ($\mathbf{H}\overline{x^b}$). The state variables were defined as follows according to state

202 augmentation method during the assimilation:

203 $\quad x_i = [c_i, \ \beta_i]^T, i = 1,2,\cdots N_{ens}$ (6)

204 $\quad c_i = [PM_{2.5}, PM_{10-2.5}, \ NO_2, \ SO_2, CO]_i$ (7)

205 $\quad \beta_i = \left[\beta_{PMF}, \beta_{BC}, \ \beta_{OC}, \ \beta_{PMC}, \beta_{NO_x}, \beta_{SO_2}, \beta_{CO}\right]_i$ (8)

206 where x_i represents the ith member of the assimilated state variable, which consists of the fields of chemical variables c_i and

207 emission perturbation factors β_i. Detailed descriptions of the model state variables are summarized in Table 1. The use of

208 PM$_{10-2.5}$ (PM$_{10}$ minus PM$_{2.5}$) values was aimed to avoid the potential cross-correlations between PM$_{2.5}$ and PM$_{10}$ (Peng et al.,

209 2018; Ma et al., 2019). Moreover, to prevent spurious correlations between non- or weakly related variables, similar to Ma et

210 al. (2019) and Miyazaki et al. (2012), state variable localization was used during assimilation, with observations of one

211 particular species only used in the updates of the same species' emission rate. Corresponding relationship between the chemical

212 observations and adjusted emissions is summarized in Table 1. The PM$_{2.5}$ observations were one exception and were used to

213 update the emissions of PMF (fine mode unspeciated aerosol), BC (black carbon) and OC (organic carbon) since the

214 observations of speciated PM$_{2.5}$ were not available in this study. The lack of speciated PM$_{2.5}$ observations may lead to

215 uncertainties in the estimated emissions of PMF, BC and OC. Therefore, we only analyzed the emissions of PM$_{2.5,}$ which were

216 the sum of the emissions of these three species. Similarly, only PM$_{10}$ emissions were analyzed in this study, which includes

217 the emissions of PM$_{2.5}$ and PMC (coarse mode unspeciated aerosol).

218 $\quad$ Due to the strict control measures implemented during the last decades, the emissions in China decreased dramatically

219 from 2010 to 2020, especially for SO$_2$. Thus, there are large biases in the a priori estimates of emissions in China (Zheng et

220 al., 2018), which would lead to incomplete adjustments of the a priori emissions and degrade the performance of assimilation.

221 Therefore, an iteration inversion scheme was developed in this study to address the large biases of SO$_2$ emissions. As illustrated

222 in Fig. 2, the main idea of the iteration inversion scheme is to update the ensemble mean of the state variable using the inversion

223 results of the kth iteration and corresponding simulations. The state variable used in the $(k+1)th$ inversions is written as

224 follows:

225 $\quad x_i^{k+1} = \left[c^k + c_i^e - \overline{c^e}, \beta^k + \beta_i^e - \overline{\beta^e}\right]^T$ (9)

226 where c^k represents the simulation results using the inversed emissions of the kth iteration, c_i^e represents the ith member of

227 ensemble simulations with an ensemble mean of $\bar{c^e}$, β^k represents the perturbation factors of the kth iteration, and

228 β_i^e represents the ith member of the ensemble of perturbation factors with a mean value of $\overline{\beta^e}$.

229   Using this method, the problems of large biases in the a priori emissions were well addressed as exemplified in Fig. 3 for

230 SO$_2$ emissions. It can be clearly seen that due to the large positive biases in the a priori SO$_2$ emissions, the model still has large

231 positive biases (NMB = 30.9–220.5%) and errors (RMSE = 8.7–23.0 μg/m^3) in simulated SO$_2$ concentration over all regions

232 of China even after assimilation (first iteration). However, the biases and errors continued to decrease with the increasing of

233 iteration times till the fourth iteration in which there were no significant improvement in SO$_2$ simulations compared to those

234 in third iteration. These results suggested that the iteration inversion method used in this study can well constrain the a priori

235 emission with large biases and, in this application, conducting three iteration is enough for constraining the emission. Besides

236 SO$_2$ emissions, the iteration inversion scheme was also applied to the emissions of other species. Meanwhile, to reduce the

237 influences of random model errors (e.g., errors in meteorological inputs) on the estimation of the variation in emissions, a 15-

238 day running average was performed on our daily inversion results after the inversion estimation.

239 **2.4 Quantification of the effects of emission changes and meteorological variations**

240   In previous studies, the meteorological-induced (MI) changes were usually determined by the CTM with a fixed emission

241 input setting and a varying meteorological input. Then, the difference between the MI changes and total changes in air pollutant

242 concentrations is defined as emission-induced (EI) changes. Another approach to estimate EI changes is to perform simulations

243 with a fixed meteorological input setting and varying emission inputs. Then, the MI changes are defined as the difference

244 between EI changes and total changes in air pollutant concentrations. Due to the nonlinear effects of atmospheric chemical

245 systems, these two methods yield different results. Thus, both methods were used in this study to account for the nonlinear

246 effects. The averaged results of these two methods are used to represent the impacts of emission changes and meteorological

247 variation on the air quality changes during the COVID-19 restrictions. In total, three scenario experiments were designed based

248 on our inversion results (Table 2). The first scenario simulation used the varying meteorological and emission inputs from the

249 P1 to P2 period, which represents the real-world scenario and is used to estimate the total changes in air pollutant concentrations

250 induced by emissions and meteorological changes from the P1 to P2 period (BASE scenario). The second scenario experiment

251 used the varying meteorological inputs but replaced the emissions during the P2 period with those during the P1 period, which

252 was used to estimate the MI changes using the first method (MET change scenario). The third scenario experiment used the

253 varying emissions input and replaced the meteorological input during the P2 period with that during the P1 period, which was

254 used to estimate the EI changes using the second method (EMIS change scenario). Based on the first method, the MI and EI

255 changes can be estimated as follows:

256 $MI_{MET\ change\ scenario} = conc_{p2,MET\ change\ scenario} - conc_{p1,MET\ change\ scenario}$ (10)

257 $EI_{MET\ change\ scenario} = conc_{p2,BASE\ scenario} - conc_{p1,BASE\ scenario} - MI_{MET\ change\ scenario}$ (11)

where $MI_{MET\ change\ scenario}$ represents the MI changes estimated based on the results from the MET change scenario, $conc_{p1,MET\ change\ scenario}$ and $conc_{p2,MET\ change\ scenario}$ represent the averaged concentrations of air pollutants during the P1 and P2 periods under the MET change scenario, $EI_{MET\ change\ scenario}$ represents the EI changes estimated based on the results from the MET change scenario, and $conc_{p1,BASE\ scenario}$, $conc_{p2,BASE\ scenario}$ respectively represent the averaged concentrations of air pollutants during the P1 and P2 periods under the BASE scenario. Similarly, the MI and EI changes estimated based on the second method are formulated as follows:

$$EI_{EMIS\ change\ scenario} = conc_{p2,EMIS\ change\ scenario} - conc_{p1,EMIS\ change\ scenario} \qquad (12)$$

$$MI_{EMIS\ change\ scenario} = conc_{p2,BASE\ scenario} - conc_{p1,BASE\ scenario} - EI_{EMIS\ change\ scenario} \qquad (13)$$

Then, the estimations from these two methods are averaged to estimate the contributions of meteorological change and emission change to the changes in $PM_{2.5}$ and O_3 concentrations during the COVID-19 lockdown:

$$MI = (MI_{EMIS\ change\ scenario} + MI_{MET\ change\ scenario})/2 \qquad (14)$$

$$EI = (EI_{EMIS\ change\ scenario} + EI_{MET\ change\ scenario})/2 \qquad (15)$$

$$contri_{met} = \frac{MI}{MI+EI} \times 100 \qquad (16)$$

$$contri_{emis} = \frac{EI}{MI+EI} \times 100 \qquad (17)$$

where $contri_{met}$ and $contri_{emis}$ represent the relative contributions (%) of the meteorological variations and emission changes to the changes in air pollutant concentrations. Detailed definition of each notation used in the calculation of MI and EI is given in Table 3.

3 Results

3.1 Validation of the inversion results

We firstly validate our inversion system by using a cross-validation method, in which 20% of observation sites were withheld from the emission inversion and used as the validation datasets. Figure S1–6 showed the concentrations of different air pollutants in China from 1st Jan to 29th Feb 2020 obtained from observations at validation sites and simulations using a priori and a posteriori emission. Commonly used statistical evaluation indices, including correlation coefficient (R), mean bias error (MBE), normalized mean bias (NMB) and root of mean square error (RMSE) are summarized in Table S1. The validation results suggest that the posteriori simulation agreed well with the observed concentrations for all species. The large biases in the a priori simulation of $PM_{2.5}$, PM_{10}, SO_2 and CO were almost completely removed in the a posteriori simulation with NMB about -3.9–15.7% for $PM_{2.5}$, -3.1–11.6% for PM_{10}, -12.6–5.3% for NO_2, -9.5–6.2% for SO_2 and -10–7.6% for CO (Table S1). RMSE values were also significantly reduced in the a posteriori simulation which were 9.1–32.2μg/m^3 for $PM_{2.5}$, 12.6–42.4μg/m^3 for PM_{10}, 5.1–12.3μg/m^3 for NO_2, 1.2–5.6μg/m^3 for SO_2 and 0.10–0.46mg/m^3 for CO. Moreover, the inversion emission considerably improved the fit to the observed time evolution of air pollutants' concentrations. The R values were

288 improved for all species in the a posteriori simulation that were up to 0.74–0.94 for $PM_{2.5}$, 0.63 – 0.92 for PM_{10}, 0.76–0.94 for
289 NO_2, 0.23–0.79 for SO_2 and 0.63–0.92 for CO. These results suggest that our inversion results have excellent performance in
290 representing the magnitude and variation of these species' emission in China during COVID-19 restrictions. Model
291 performance in simulating O_3 concentration is relatively poor compared to other species although improvement was
292 remarkable in NCP, NE and SE regions. This would be due to the use of outdated emission inventory for base year 2010 and
293 that the emission of non-mental volatile organic compounds (NMVOC), another important precursor for O_3, were not
294 constrained in this study. As shown in fig. S7, the NMVOC emissions for base year 2010 were generally lower than those for
295 2018 except over the SW regions. Considering the increasing trend of NMVOC emissions in China (Li et al., 2019), the
296 underestimates of NMVOC emissions for base year 2020 could be larger. This is in line with the negative biases in the
297 simulated O_3 concentrations over these regions.

3.2 Emission changes of multi-species during COVID-19 restrictions

3.2.1 Unbalanced emission changes between NO_x and other species

300 The control of COVID-19 began on 23rd January when the Chinese government declared the first level of national
301 responses to public health emergencies, one day before the 2020 Chinese New Year Eve. Figure 4 shows the time evolution
302 of the normalized emission anomaly for different species in China from 1st January to 29th February. The temporal variation
303 in the emission varied largely between NO_x and other species. Due to the combined effects of the Spring Festival and COVID-
304 19 lockdown, NO_x emissions decreased continuously at the beginning of January until approximately one week after the
305 implementation of the COVID-19 lockdown, with estimated decreases in NO_x emissions of up to 42.5% from the P1 to P2
306 period (Table 4). Subsequently, the NO_x emissions stabilized with small fluctuations until the official back-to-work day when
307 the NO_x emissions began to increase due to easing of the control measures and the resumption of business. According to
308 inversion estimation, NO_x emissions recovered by 3.9% during the P3 period. These results indicate that the temporal variation
309 in our estimated NO_x emissions agreed well with the timing of the Spring Festival and different control stages of COVID-19.
310 However, for other species (i.e., $PM_{2.5}$, PM_{10}, SO_2 and CO), although their emissions generally decreased from 1st January to
311 the end of the 2020 Spring Festival holiday, they showed much smaller reductions than the NO_x emissions. The emission
312 reduction for these species was only approximately 7.9-12.1% (Table 4). This is consistent with the inversion results by Hu et
313 al. (2022) who found that SO_2 emissions in China decreased only by 9.2% during COVID-19 lockdown. In addition, the
314 emissions of these species quickly rebounded to their normal level just one week after the end of the Spring Festival holiday.
315 As estimated by our inversion results, the SO_2 emissions recovered by 7.2% during the P3 period, which was only 2.5% lower
316 than that during the P1 period. The $PM_{2.5}$ and PM_{10} emissions during the P3 period were 3.3% and 43.6% higher, respectively,
317 than those during the P1 period.
318 Similar results were found in different regions of China (Fig. 5 and Table 5), where the NO_x emissions decreased much
319 more than other species. In addition, unlike the uniform decreases in NO_x emissions in different regions of China (~40%),

320   there was apparent spatial heterogeneity in the emission changes in $PM_{2.5}$, PM_{10}, SO_2 and CO (Table 5 and Fig. 6). For example,

321   from the P1 to P2 period, the $PM_{2.5}$ emissions decreased by over 20% in the Central region but only by 8.8% in the NE region.

322   The $PM_{2.5}$ emissions even increased by 5.5% in the NCP region. This may be due to the increased emissions from industry

323   and fireworks according to the field measurements conducted by previous studies (Li et al., 2022; Ma et al., 2022; Zuo et al.,

324   2022; Dai et al., 2020). Based on the measurement of stable Cu and Si isotopic signature and distinctive metal ratios in Beijing

325   and Hebei, Zuo et al. (2022) analyzed the variations in the $PM_{2.5}$ sources during the COVID-19 pandemic, who reported that

326   the primary $PM_{2.5}$ emissions did not decrease in Beijing and Hebei, and that the PM-associated industrial emissions may

327   actually increase during the lockdown period. The increased industrial heat sources detected by Li et al. (2022) based on VIIRS

328   active fire data also supported the increased industrial emissions over the NCP region during lockdown period. Meanwhile,

329   consistent with the field measurements in Beijing and Tianjin conducted by Ma et al. (2022) and Dai et al. (2020), substantial

330   high levels of potassium (K^+) and magnesium (Mg^{2+}) ion were found over the NCP region during the Spring Festival according

331   to the aerosol chemical composition measurements obtained from CNEMC (Fig. S8). Since K^+ and Mg^{2+} are two important

332   fingerprints of the firework emissions, the high levels of K^+ and Mg^{2+} suggest that the emissions from fireworks during Spring

333   Festival were also a potential contributor to the increased of $PM_{2.5}$ emissions over the NCP region. In contrast, the SW and

334   central regions exhibited relatively larger emission reductions for these species (Fig. 5 and Table 5) by 12.6–25.9% and 10.6–

335   23.7%, respectively. The emission rebound during the P3 period was more prominent in the SE, central and SW regions (Fig.

336   5 and Fig. 7), where emissions recovered by 6.0–16.4% for NO_x, 7.5–19.8% for SO_2, 7.4–13.1% for CO, 12.3–47.7% for $PM_{2.5}$

337   and 28.6–135.9% for PM_{10} (Table 5). This result is consistent with the earlier degradation of the response level to the COVID-

338   19 virus (from the first level to the second or third level) over these regions (Table S2). In contrast, there were decreases in

339   emissions in the NCP, NE and NW regions. $PM_{2.5}$ emissions were reduced by 9.9% in the NCP region and by 19.2% in the

340   NE region from the P2 to P3 period (Table 5). Moreover, we found that the PM_{10} emissions surged in the NW and central

341   regions, where the PM_{10} emissions during the P3 period were almost two times larger than those during the P2 period (Table

342   5). However, this finding may be related to the enhanced dust emissions over these two regions rather than the effects of

343   returning to work according to the decreased $PM_{2.5}/PM_{10}$ ratios during the P3 period. According to Fig.S9, the $PM_{2.5}/PM_{10}$

344   ratio was relatively stable during the P1 and P2 period, but it decreased substantially during the P3 period, from 0.81 to 0.48

345   over the NW region and from 0.77 to 0.53 over the Central region. A lower $PM_{2.5}/PM_{10}$ ratio commonly suggests that the PM_{10}

346   is more likely to be attributed to natural sources such as dust (Wang et al., 2015; Fan et al., 2021). Moreover, the NW and

347   Central region are typical source areas of dust in China, therefore the increasing of PM_{10} emissions over NW and Central

348   regions may be mainly related to the enhanced dust emissions. This demonstrates the necessity to consider changes in natural

349   emissions during COVID-19 restrictions. Thus, to reduce the effects of natural emissions on our findings, the same analysis

350   was performed for the emissions over southeast China (Fig. S10) where emissions were dominated by anthropogenic sources,

351   which shows consistent results with the findings above (Fig. S11 and Table S3).

3.2.3 Explanations for the emission changes during COVID-19 restrictions

Two explanations may help clarify the unbalanced emission changes between NO_x and other species. First, the COVID-19 lockdown policy has led to dramatic decreases in transportation activities throughout China; however, as shown in Fig. 4, the relative contributions of the transportation sector to the emissions of SO_2 (2.4%), CO (18.5%), $PM_{2.5}$ (6.1%) and PM_{10} (4.7%) are much smaller than those for NO_x emissions (34.3%) (Zheng et al., 2018; Li et al., 2017a). Thus, the reduction in traffic activities can only substantially decrease NO_x emissions. Reductions in CO emissions (-10.6%) were relatively larger than those for SO_2 (-9.7%) and $PM_{2.5}$ (-7.9%) emissions, which is consistent with the relatively larger contributions of the transportation sector to CO emissions. However, the differences in the percentage decreases in emissions of CO, SO_2 and $PM_{2.5}$ is not as significant as the differences in their transportation share (18% versus 2% and 6%). This may be on the one hand due to the uncertainty in the estimated relative contributions of different sectors to the total emissions of CO, SO_2 and $PM_{2.5}$, on the other hand were possibly due to the uncertainty in the emission inversions, especially considering that the decreasing trend of CO, SO_2 and $PM_{2.5}$ were not significant. Also, other factors beyond transportation may have influenced the reductions of anthropogenic emissions during P2 period. For example, the PM_{10} emissions showed the largest reductions among these four species, which is related in part to the reduced dust emissions due to shutting down of construction sites during the lockdown period (Li et al., 2020). Second, as shown in Fig. 4, the industrial and residential sectors are the major contributors to the anthropogenic emissions of SO_2, CO, $PM_{2.5}$ and PM_{10} in China, together contributing 77.6%, 78.3%, 86.5% and 86.3%, respectively, to their total emissions. The much smaller reductions of these species' emissions were thus in line with the fact that there were no intentional restrictions on heavy industry during the COVID-19 restrictions. A large number of non-interruptible processes, such as steel, glass, coke, refractory, petrochemical, electric power, and especially heating, cannot be stopped during the COVID-19 lockdown. According to statistical data from the National Bureau of Statistics of China (Fig. S12), the industrial and power sectors did not show similar reductions in their activity levels as those seen in the transportation sector. Power generation and steel production even showed increases in many provinces, which corresponds well with the emission increases over these regions. In addition, since people were required to stay at home, residential emissions were likely increased due to the increased energy consumption for heating or cooking. Therefore, our inversion results supported the views that the emissions of species related to industrial and residential activities did not decline much during the lockdown period, and that the COVID-19 lockdown policy was largely a traffic control measure with small influences on other sectors.

3.3 Investigation of air quality change over the NCP region during COVID-19 restrictions

Using the inversion results, we reassessed the environmental impacts of the COVID-19 restrictions on the air pollution over NCP region. The NCP region was chosen because it is the key target region of air pollution control in China and where unexpected severe haze occurred. A major caveat in previous studies that explored the impacts of COVID-19 lockdowns on air quality is the uncertainty in the emission changes during COVID-19 restrictions. The inversion results enable us give a more reliable assessment of the environmental impacts of COVID-19 restrictions. Figure 8 shows the observed changes in

PM2.5 and O3 concentrations over the NCP region from the P1 to P2 period. The observations showed consistent reductions in PM2.5 concentrations over the NCP region (by 13.6 μg/m³). However, substantial increases in PM2.5 concentrations were observed in the Beijing area (by 31.2 μg/m³). In contrast to the widespread reductions in PM2.5 concentrations, the O3 concentrations significantly increased over the whole NCP region (by 28.3 μg/m³) and the Beijing area (by 16.8 μg/m³). The simulations based on our inversion results reproduced the observed changes in PM2.5 and O3 concentrations over the NCP region well, although the O3 concentrations were underestimated in all regions (Fig. S6) and the changes in PM2.5 and O3 concentrations were slightly overestimated by 1.6 and 2.6 μg/m³ in the simulation (Fig. 8).

As detailed in the Sect 2.4, the simulated changes in air pollutant concentrations before and after lockdown were decomposed into meteorological-induced (MI) changes and emission-induced (EI) changes through two different scenarios to account for the nonlinearity of the atmospheric chemical system. According to Fig. S13, the differences in calculated MI and EI based on different scenarios were small for PM2.5 concentrations, which were about 2 μg/m³ in this application, while they were relatively larger for O3, which were around 5 μg/m³ over the Beijing and NCP region (Fig. S14). In addition, the sign of calculated MI using different scenarios were opposite although both suggested weak contributions of meteorological variation to the changes of O3 concentrations. This suggests that the calculated MI and EI changes of O3 concentrations could be more sensitive to the used scenarios, which may be associated with the stronger chemical nonlinearity of the O3 concentrations. Figure 9 shows the mean results of the calculated MI and EI changes using the two different scenarios. It shows that the meteorological variation dominated the changes in PM2.5 concentrations over the NCP region, which contributed 90% of the PM2.5 reductions over most parts of the NCP region. Moreover, this variation made significant contributions (57.9%) to the increases in PM2.5 concentrations over the Beijing area. This finding suggested that meteorological variations played an irreplaceable role in the occurrence of the unexpected PM2.5 pollution around the Beijing area. Compared with the meteorological conditions before lockdown (Fig. 10), there were increases in relative humidity over northern China, which facilitated the reactions for aerosol formation and growth. Wind speed also decreased over the Beijing area accompanied by an anomalous south wind, which facilitated aerosol accumulation and the transportation of air pollutants from the polluted industrial regions of the Hebei Province to Beijing. The increases in boundary layer height from the P1 to P2 period were also much smaller in the Beijing area than in other areas of the NCP. Thus, the Beijing area has exhibited distinct meteorological variations from other areas of the NCP region, which correspond well to the different changes in PM2.5 concentrations over the Beijing area.

The emission changes contributed slightly to the PM2.5 reductions over the NCP region (8.6%). This is because, on the one hand, the large reductions in NO$_x$ emissions (by 44.4%) only reduced nitrate by approximately 10–30% due to the nonlinear effects of chemical reactions (Fig. 11), and on the other hand, the emissions of primary PM2.5 and its precursors from other sectors changed little during the COVID-19 restrictions (Table 5). The emission changes contributed more to the increased PM2.5 concentrations over the Beijing area (42.1%). This is mainly associated with the increases in primary PM2.5 emissions around the Beijing area, as seen in Fig. 6, possibly due to the increased emissions from the industry as we mentioned before (Zuo et al., 2022) and the increased firework emissions during the Spring Festival as shown by the rapid increases in

concentrations of K^+ and Mg^{2+} measured by CNEMC (Fig. S15). Therefore, our results suggested that the unexpected $PM_{2.5}$ pollution during lockdown period was mainly driven by unfavorable meteorological conditions together with small changes or even increases in primary $PM_{2.5}$ emissions. This finding is in line with previous results of Le et al. (2020) but different from those of Huang et al. (2021), who suggested that enhanced secondary aerosol formation was the main driver of severe haze during the COVID-19 restrictions. To investigate it, we further analyzed the changes in the concentrations of secondary inorganic aerosols (SIAs). First, we evaluated our model results against the observed SIA concentrations, which showed that the model results using our inversion emissions well reproduced the observed concentrations of SIAs over the NCP region (Fig. 12) with mean bias (MB) ranging from -5.14 to 5.45 $\mu g/m^3$ and correlation coefficient (R) ranging from 0.59 to 0.80. The observed increases in SIA concentrations over the Beijing area, especially for sulfate concentrations, were also captured in our simulations (Fig. 11), although underestimation occurred due to the uncertainty in simulating SIA concentrations. Through sensitivity experiments, we found that the increases in SIA concentrations were still driven by meteorological variations (Fig. 13). In fact, the emission reductions only led to a 10% decrease in SIA concentrations over the NCP region. This finding suggests that the enhanced secondary aerosol formation was likely mainly driven by the unfavorable meteorological conditions associated with higher temperature and relative humidity instead of the emission reductions during the lockdown period. This is in line with the observation evidences from Ma, T et al (2022) who emphasized that the increased temperature and relative humidity promoted the formation of secondary pollutants during the COVID-19 restrictions.

In terms of O_3 concentrations, the emission changes subsequently became the dominant contributor to the O_3 increases by more than 100% in the Beijing area and by 96.0% over the NCP region. This result is mainly because the lockdown period occurred in midwinter when photochemical O_3 formation was minimal; thus, the large increase in O_3 is expected solely from the effect of the reduced titration reaction associated with the large reductions in NO_x emissions. Although the higher temperature and slower wind speed during the lockdown period were favorable for the increases in O_3 concentrations, their contributions were much smaller than those of emission changes (Fig. 9). These results suggested that control measures, such as COVID-19 restrictions, were inefficient for air pollution mitigation in China considering the high economic cost of the COVID-19 restrictions.

We also compared our results with previous studies that differentiated the contributions of meteorology and emission to the $PM_{2.5}$ and O_3 concentrations. Before comparisons, it should be noted that it is difficult to directly compare our results with previous studies due the altered definition of meteorological contribution, different reference period that used to quantify the meteorological contributions and different targeted region. For example, in Song et al. (2021), the reference period used to determine the meteorological contribution is the corresponding period of COVID-19 pandemic in 2019. Le et al. (2020) used the multiyear climatology as the reference period. In Wang et al. (2020) and Sulaymon et al. (2021), the MI changes of $PM_{2.5}$ concentrations were defined as the difference between the modeled concentrations in high-pollution days and those in low-pollution days under hypothetical emission reduction scenario. Zhao et al. (2020) used a similar reference period to ours to determine the MI changes but they used the outdated emission inventory. Table 6 summarized the results from the selected studies over Beijing and Beijing-Tianjin-Hebei region. Note that some studies only provided the relative changes in the

modeled PM$_{2.5}$ concentrations. It shows that due to the uncertainties in emission changes during COVID-19 pandemic, the EI changes estimated by Zhao et al. (2020) were possibly overestimated compared to our studies (55% versus 24.7%). Both Sulaymon et al. (2021) and Wang et al. (2020) suggested negative EI changes during COVID-19 period in Beijing. This because they presumed that the emissions were largely reduced during COVID-19 lockdown which may deviate from the real changes of emissions according to our inversion results. Meanwhile, although they used same method and reference period, their results differed largely (-2.7 versus -13.4 $\mu g/m^3$) due to the different emission reduction scenario they assumed. Le et al. (2020) only considered the emission reductions of NO$_x$ in their sensitivity simulations without considerations of other species, therefore their calculated EI changes may be underestimated compared to our results (almost 0% versus 24.7%). However, the calculated MI changes were consistent between our study and Le et al. (2020). In terms of O$_3$, the calculated EI changes by our study were also higher than that calculated by Zhao et al. (2020) in Beijing (85.7% versus 70%). These results suggested that the EI and MI changes calculated by our study could be more reasonable, considering that the emissions of different species were well constrained which could better represent the temporal variation and spatial heterogeneity of emission changes during COVID-19.

4 Conclusions and discussions

The COVID-19 pandemic is an unprecedented event that significantly influenced the social activity and associated emissions of air pollutants. Our results provide a quantitative assessment of the influences of COVID-19 restrictions on multi-air pollutant emissions in China. Otherwise, understanding of the relationship between air quality and human activities may be biased. The inversion results provide important evidences that the COVID-19 lockdown policy was largely a traffic control measure with substantially reducing impacts on NO$_x$ emissions but much smaller influences on the emissions of other species and other sectors. Traffic control has widely been considered to be the normal protocol in implementing regulations in many cities of China, but its effectiveness on air pollution control is still disputed (Han and Naeher, 2006; Zhang et al., 2007; Chen et al., 2021; Cai and Xie, 2011; Chowdhury et al., 2017; Li et al., 2017c). Thus, the COVID-19 restrictions provided us with a real nationwide traffic control scenario to investigate the effectiveness of traffic control on the mitigation of air pollution in China. The results suggested that traffic control as a separate pollution control measure has limited effects on the coordinated control of high concentrations of O$_3$ and PM$_{2.5}$ under the current air pollution conditions in China. In this case, the PM$_{2.5}$ concentrations were slightly reduced, while leading to substantial increases in O$_3$ concentrations. Severe haze was also not avoided during the COVID-19 restrictions due to unbalanced emission changes from other sectors and unfavorable meteorological conditions. China is now facing major challenges in both controlling PM$_{2.5}$ and controlling emerging O$_3$ pollution. The tragic COVID-19 pandemic has revealed the limitation of the road traffic control measure in the coordinated control of PM$_{2.5}$ and O$_3$. More comprehensive regulations for multiple precursors from different sectors are required in the future to address O$_3$ and PM$_{2.5}$ pollution in China.

Finally, there are certain limitations that should be aware of in our inversion work. Firstly, the COVID-19 restrictions were initiated during the Spring Festival of China which would also influence the air pollutant emissions in China. However, the inversion method used in this study did not differentiate the contributions of the Spring Festival from the COVID-19 restrictions. Similarly, the effects of natural emission changes were not differentiated in this study, which would lead to uncertainty in quantifying the effects of the COVID-19 restrictions on air pollutant emissions. Secondly, the overestimations of NO_2 measurement induced by chemiluminescence monitor interference were not directly corrected in our study due to the lack of synchronous observations of HNO_3, PAN and AN, thus the estimated NO_x emissions could be slightly overestimated according to the sensitivity run with corrected NO_2 measurement using CFs (Fig. S16–18). Meanwhile, the sensitivity results suggest that the inversed NO_x emissions may even drop faster if the NO_2 measurement were corrected over the SE and SW regions (Fig. S19). Thirdly, the use of outdated emission inventory as the a priori emission would also be a potential limitation in our work although the iteration inversion method was used. A sensitivity inversion run was thus conducted based on the a priori emission for a more recent year of 2018 to test the influence of the a priori emission inventory. This new emission inventory is comprised of the anthropogenic emissions obtained from HTAPv3 (Crippa et al., 2023), the biogenic, soil and oceanic emissions obtained from the CAMS global emission inventory (https://ads.atmosphere.copernicus.eu/cdsapp#!/dataset/cams-global-emission-inventories?tab=overview, last access: March 15, 2023) and the biomass burning emissions obtained from the Global Fire Assimilation System (GFAS) (Kaiser et al., 2012). Detailed steps of the new inversion estimation were same as those elucidated in Sect.2. The results suggest that the inversion results based on the 2010 and 2018 inventory were broadly close to each other, while the inversion results based on 2018 inventory were relatively higher than those based on 2010 inventory, reflecting the uncertainty in our inversion results caused by the choice of a priori emission inventory (Fig. S20–22). However, the sensitivity run consistently showed that the NO_x emissions decreased much larger than other species (Fig. S23–24). This suggests that the choice of a priori emission inventory may not obviously influence the main conclusion of our study, but can lead to uncertainty in the magnitude of the inversion results which should be aware of by potential readers.

517 **Tables**

518 **Table 1. Corresponding relationship between the chemical observations and adjusted emissions**

Species	Descriptions	Observations that used for inversions of this species
BC	black carbon	$PM_{2.5}$
OC	organic carbon	$PM_{2.5}$
PMF	fine mode unspeciated aerosol	$PM_{2.5}$
PMC	coarse mode unspeciated aerosol	$PM_{10} - PM_{2.5}$
NO_x	nitrogen oxide	NO_2
SO_2	sulfur dioxide	SO_2
CO	carbon monoxide	CO

519

520 **Table 2. Configuration of simulation scenarios**

Scenarios	Meteorology input	Emission input	Purpose
BASE scenario	varied meteorological condition from pre lockdown to lockdown period	varied emission from pre-lockdown to lockdown period	To estimate the total changes of air pollutant concentrations induced by emission and meteorological change
MET change scenario	varied meteorological condition from pre-lockdown to lockdown period	constant emissions during pre-lockdown and lockdown period	To estimate the impacts of meteorological changes on the air pollutants
EMIS change scenario	constant meteorological during pre-lockdown and lockdown period	varied emission from pre-lockdown to lockdown period	To estimate the impacts of emission changes on the air pollutants

521
522
523
524
525
526
527

528

Table 3. Descriptions of different items used in the calculation of meteorological-induced and emission-induced changes of air pollutant concentrations

notation	description
MI	meteorological-induced changes in air pollutant concentrations
EI	emission-induced changes in air pollutant concentrations
$MI_{MET\ change\ scenario}$	meteorological-induced changes in air pollutant concentrations calculated by the MET change scenario
$EI_{MET\ change\ scenario}$	emission-induced changes in air pollutant concentrations calculated by total changes minus $MI_{MET\ change\ scenario}$
$EI_{EMIS\ change\ scenario}$	emission-induced changes in air pollutant concentrations calculated by the EMIS change scenario
$MI_{EMIS\ change\ scenario}$	meteorological-induced changes in air pollutant concentrations calculated by total changes minus $EI_{EMIS\ change\ scenario}$
$conc_{p1,BASE\ scenario}$	averaged concentrations of air pollutants during P1 period under the BASE scenario
$conc_{p2,BASE\ scenario}$	averaged concentrations of air pollutants during P2 period under the BASE scenario
$conc_{p1,MET\ change\ scenario}$	averaged concentrations of air pollutants during P1 period under the MET change scenario
$conc_{p2,MET\ change\ scenario}$	averaged concentrations of air pollutants during P2 period under the MET change scenario
$conc_{p1,EMIS\ change\ scenario}$	averaged concentrations of air pollutants during P1 period under the EMIS change scenario
$conc_{p2,EMIS\ change\ scenario}$	averaged concentrations of air pollutants during P2 period under the EMIS change scenario
$contri_{met}$	relative contributions of the meteorological variations to the changes in air pollutant concentrations
$contri_{emis}$	relative contributions of the emission changes to the changes in air pollutant concentrations

531

532

533

534

535

Table 4. Inversion estimated emissions of different air pollutants in China and their changes between different periods during COVID-19.

	NO_x	SO_2	CO	$PM_{2.5}$	PM_{10}
P1 (Gg/day)	72.9	23.8	1160.2	44.5	75.5
P2 (Gg/day)	41.9	21.5	1037.4	40.9	66.4
P3 (Gg/day)	44.8	23.2	1078.2	45.9	108.4
(P2-P1)/P1	-42.5%	-9.7%	-10.6%	-7.9%	-12.1%
(P3-P2)/P1	3.9%	7.2%	3.6%	11.2%	55.7%
(P3-P1)/P1	-38.6%	-2.5%	-7.0%	3.3%	43.6%

561 **Table 5. Inversion estimated emission changes of different air pollutants over different regions in China between different periods**
562 **during COVID-19 restrictions**

	NO_x	$PM_{2.5}$	PM_{10}	SO_2	CO
NCP					
(P2-P1)/P1	-44.4%	5.5%	2.8%	-1.6%	-4.3%
(P3-P2)/P1	-0.8%	-9.9%	31.8%	-5.9%	-10.0%
(P3-P1)/P1	-45.2%	-4.3%	34.7%	-7.5%	-14.3%
NE					
(P2-P1)/P1	-41.8%	-8.8%	-3.5%	-3.2%	-10.9%
(P3-P2)/P1	-6.0%	-19.2%	23.7%	-2.9%	-6.6%
(P3-P1)/P1	-47.8%	-28.0%	20.2%	-6.1%	-17.5%
SE					
(P2-P1)/P1	-41.4%	-9.5%	-24.4%	-19.4%	-3.5%
(P3-P2)/P1	10.2%	12.3%	28.6%	19.8%	13.1%
(P3-P1)/P1	-31.2%	2.8%	4.2%	0.3%	9.7%
SW					
(P2-P1)/P1	-43.5%	-12.6%	-25.9%	-17.5%	-23.8%
(P3-P2)/P1	6.0%	47.7%	33.1%	7.5%	7.4%
(P3-P1)/P1	-37.5%	35.1%	7.2%	-10.0%	-16.4%
NW					
(P2-P1)/P1	-38.5%	-4.0%	-8.3%	14.2%	-2.6%
(P3-P2)/P1	-21.1%	4.9%	145.3%	-4.1%	-7.2%
(P3-P1)/P1	-59.6%	0.9%	136.9%	10.1%	-9.8%
Central					
(P2-P1)/P1	-43.8%	-23.7%	-15.7%	-10.6%	-17.4%
(P3-P2)/P1	16.4%	24.4%	135.9%	18.5%	8.4%
(P3-P1)/P1	-27.4%	0.7%	120.3%	7.9%	-9.0%

563

564

565

566 **Table 6. Calculated MI and EI changes in PM$_{2.5}$ concentrations during COVID-19 pandemic by previous studies**

	MI changes	EI changes	Region	Reference period	Method	Reference
1	26.79 µg/m^3	-21.84 µg/m^3	Beijing	January 23-March 10, 2019 versus January 23-March 10, 2020	observation-based wind-decomposition method	Song et al. (2021)
2	Around 20 µg/m^3	-2.7 µg/m^3	Beijing	January 01 to February 29, 2020	CTM with hypothetical emission reduction scenario	Sulaymon et al. (2021)
3	Around 45 µg/m^3	-13.4 µg/m^3	Beijing	January 01 to February 29, 2020	CTM with hypothetical emission reduction scenario	Wang et al. (2020)
4	31.3%	Around 0%	Beijing-Tianjin-Hebei	January 01 to February 13, 2020	CTM sensitivity simulations using different emission rates and multiyear climatology	Le et al. (2020)
5	Around 5%	Around 55%	Beijing	January 16-22, 2020 versus January 26 to February 1, 2020	CTM with fixed emission inventory for 2017	Zhao et al. (2020)
6	17.5 µg/m^3 (34.0%)	12.7 µg/m^3 (24.7%)	Beijing	January 1-20, 2020 versus January 21 to February 9, 2020	CTM with inversion emission inventory	This study

567

568   **Figures**
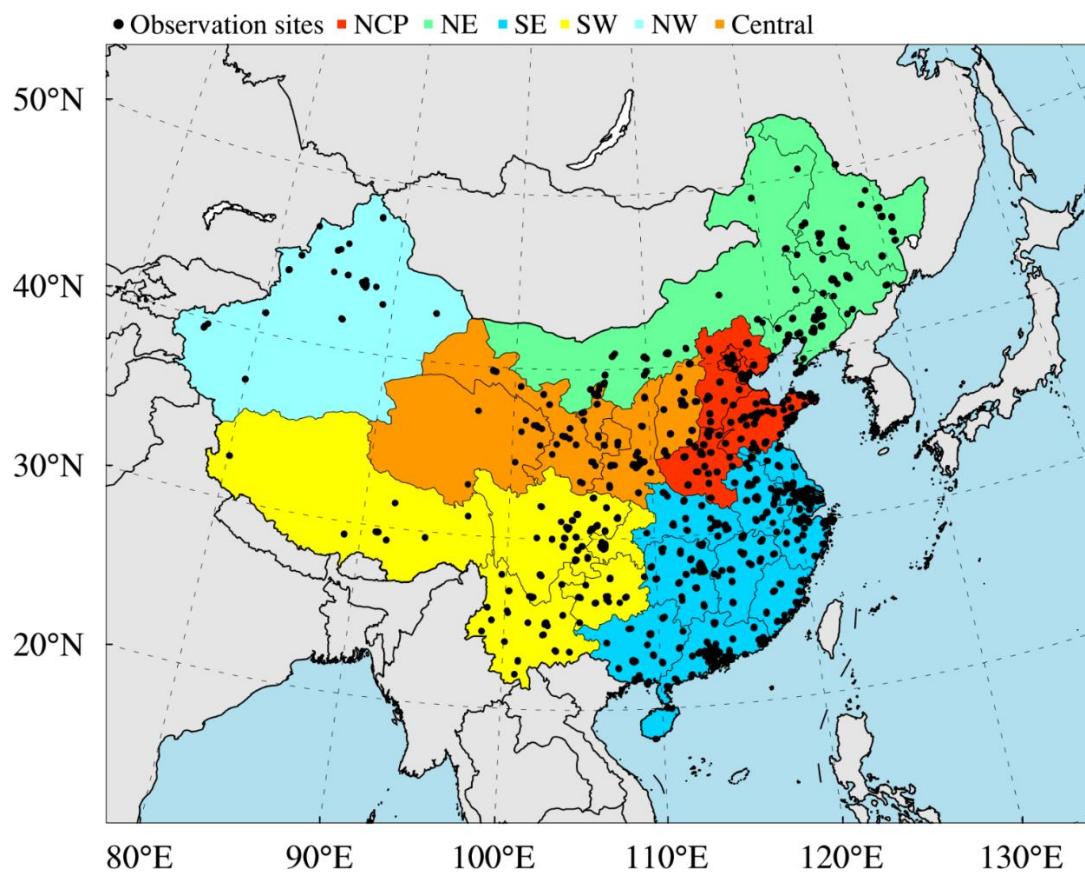
569

570   **Figure 1: Modeling domain of the ensemble simulation overlay the distributions of observation sites from CNEMC. Different colours**
571   **denote the different regions in mainland of China, namely North China Plain (NCP), Northeast China (NE), Southwest China (SW),**
572   **Southeast China (SE), Northwest China (NW) and Central.**
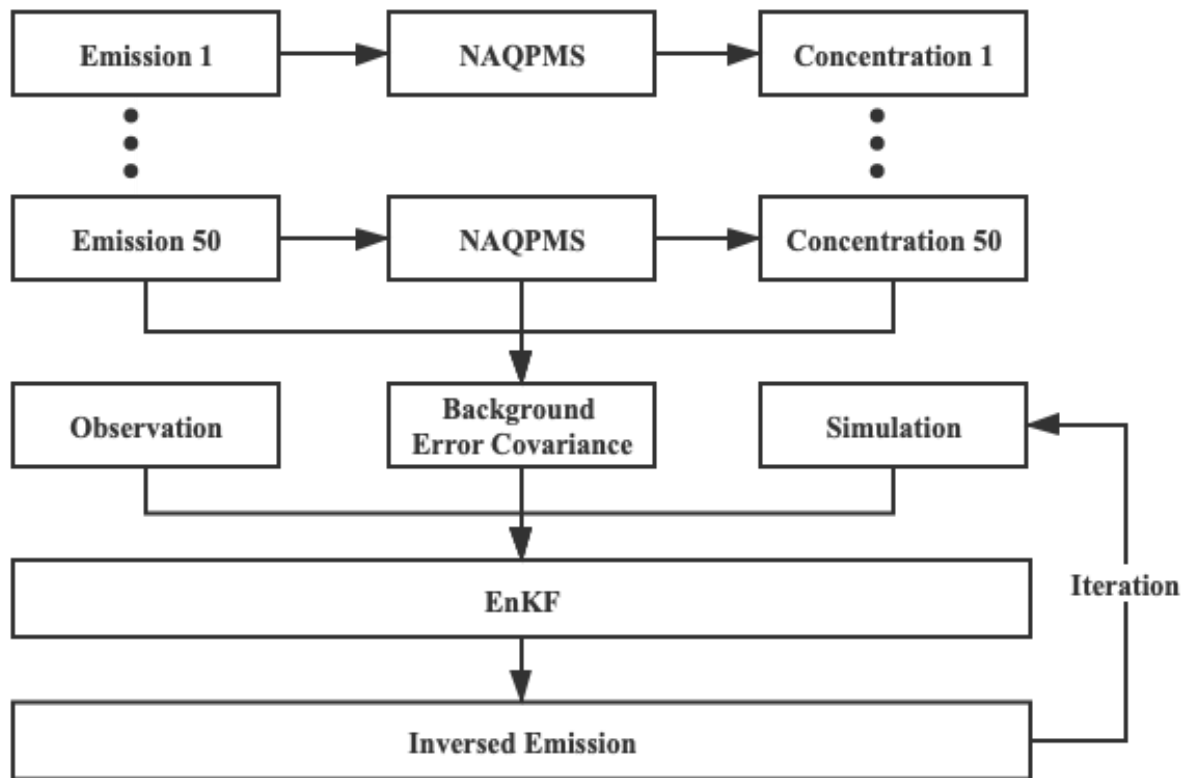
573

574   **Figure 2: Illustration of the iteration inversion scheme used in this study.**

575
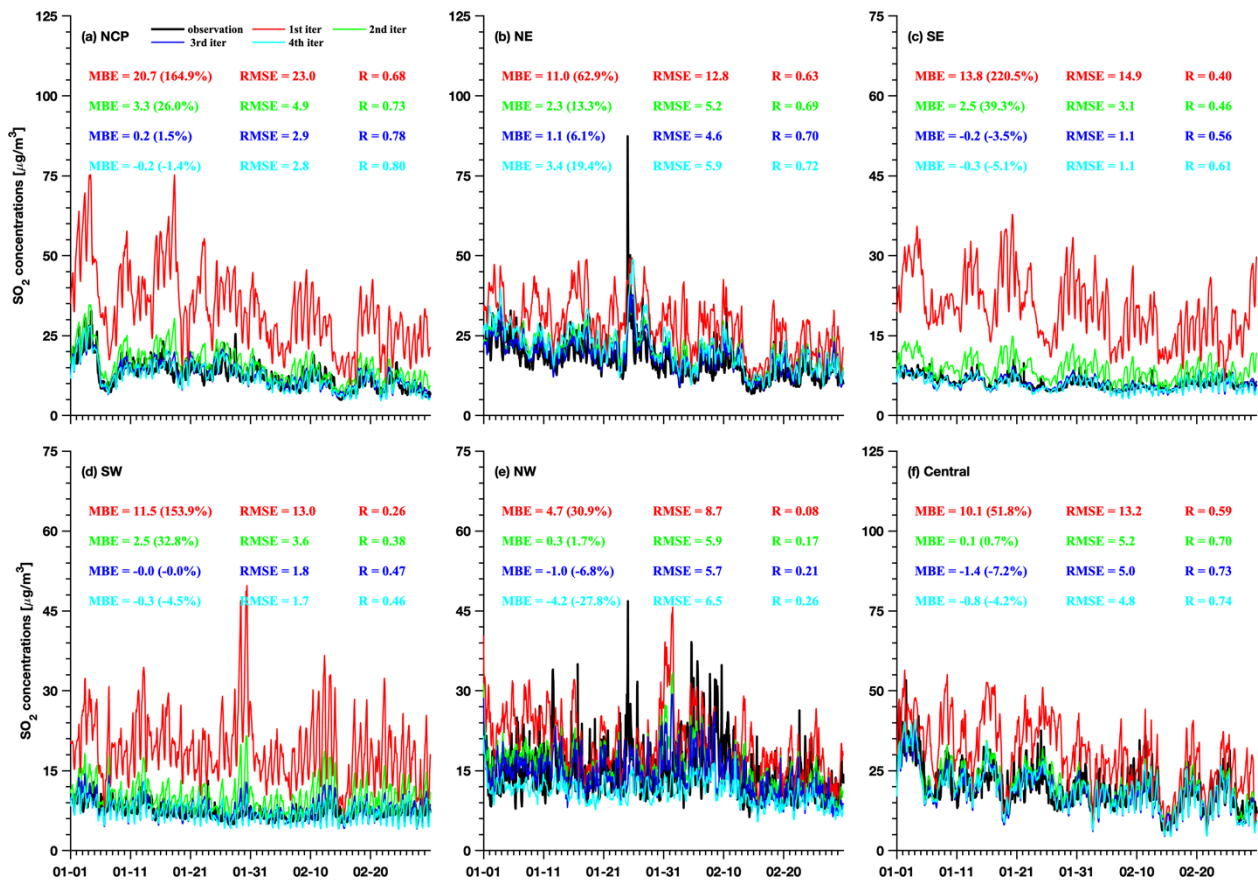
Figure 3: Comparisons of the observed and simulated mean SO₂ concentrations using emissions of different iteration time at validation sites over (a) NCP region, (b) NE region, (c) SE region, (d) SW region, (e) NW region and (f) Central region.
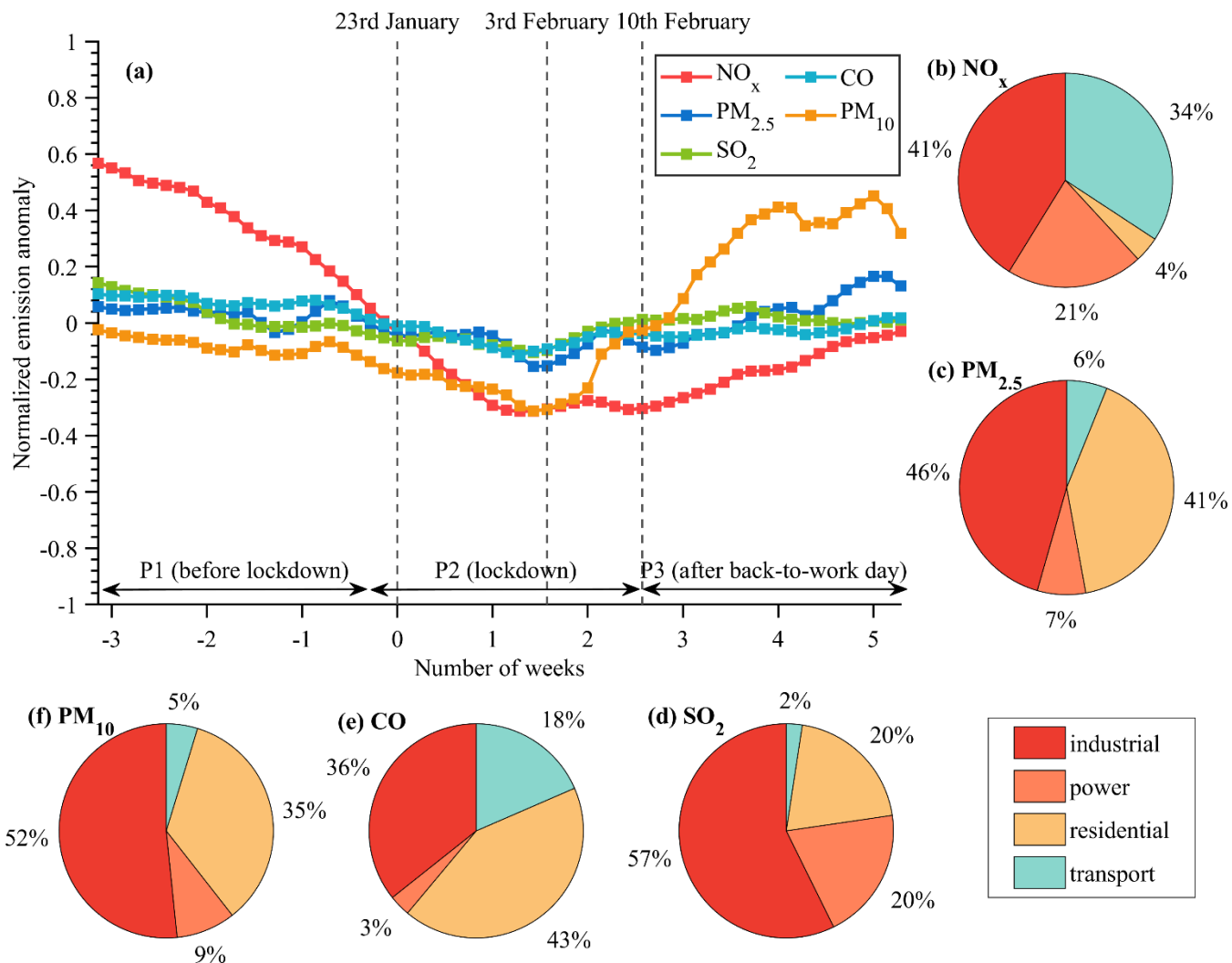
581
582
583 Figure 4: (a) Time series of normalized emission anomalies estimated by inversion results for different species in China from 1st
584 January to 29th February 2020, and (b-f) Relative contributions of different sectors to the total anthropogenic emissions of NO_x,
585 $PM_{2.5}$, PM_{10}, CO and SO_2 obtained from Zheng et al. (2018). The normalized emission anomaly is calculated by the emission anomaly
586 divided by the average emissions during the whole period.
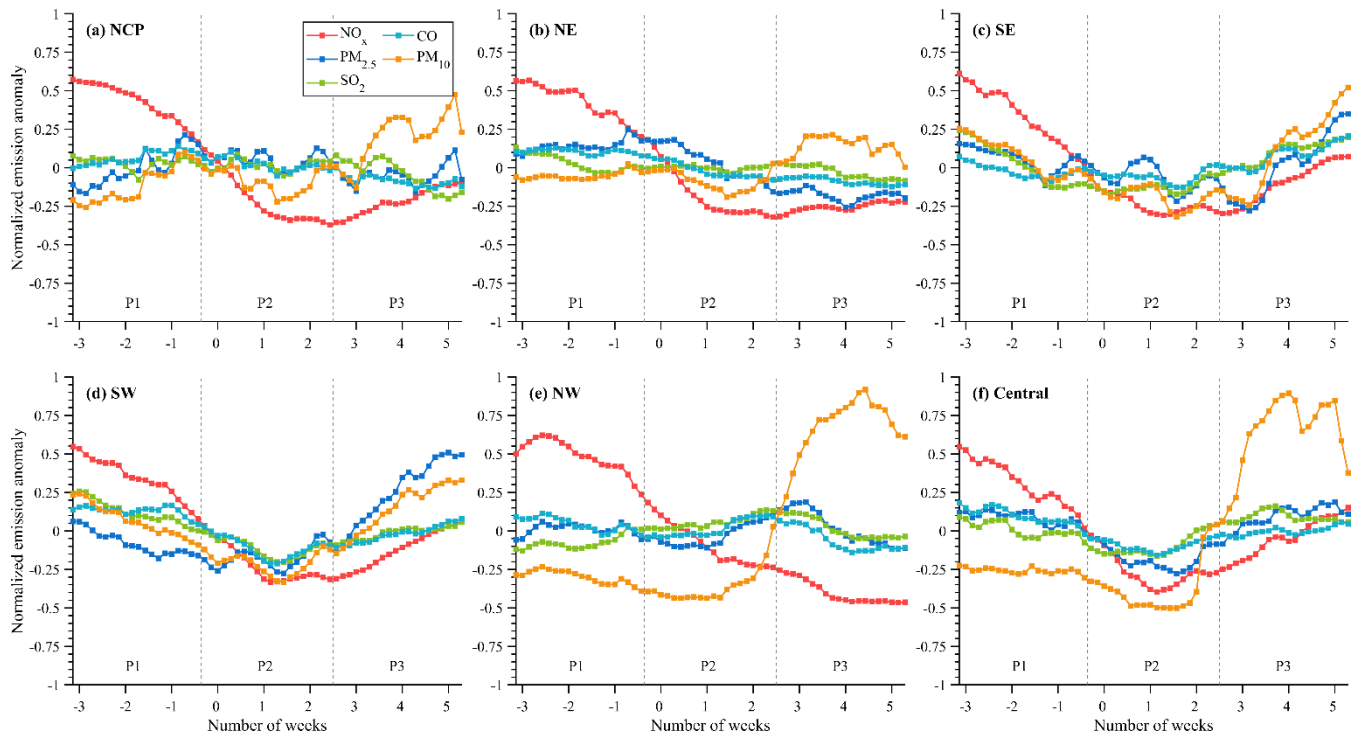
587
588 **Figure 5: Time series of normalized emission anomalies estimated by inversion results for different species over (a) NCP region, (b)**
589 **NE region, (c) SE region, (d) SW region, (e) NW region and (f) Central region from 1st January to 29th February 2020.**
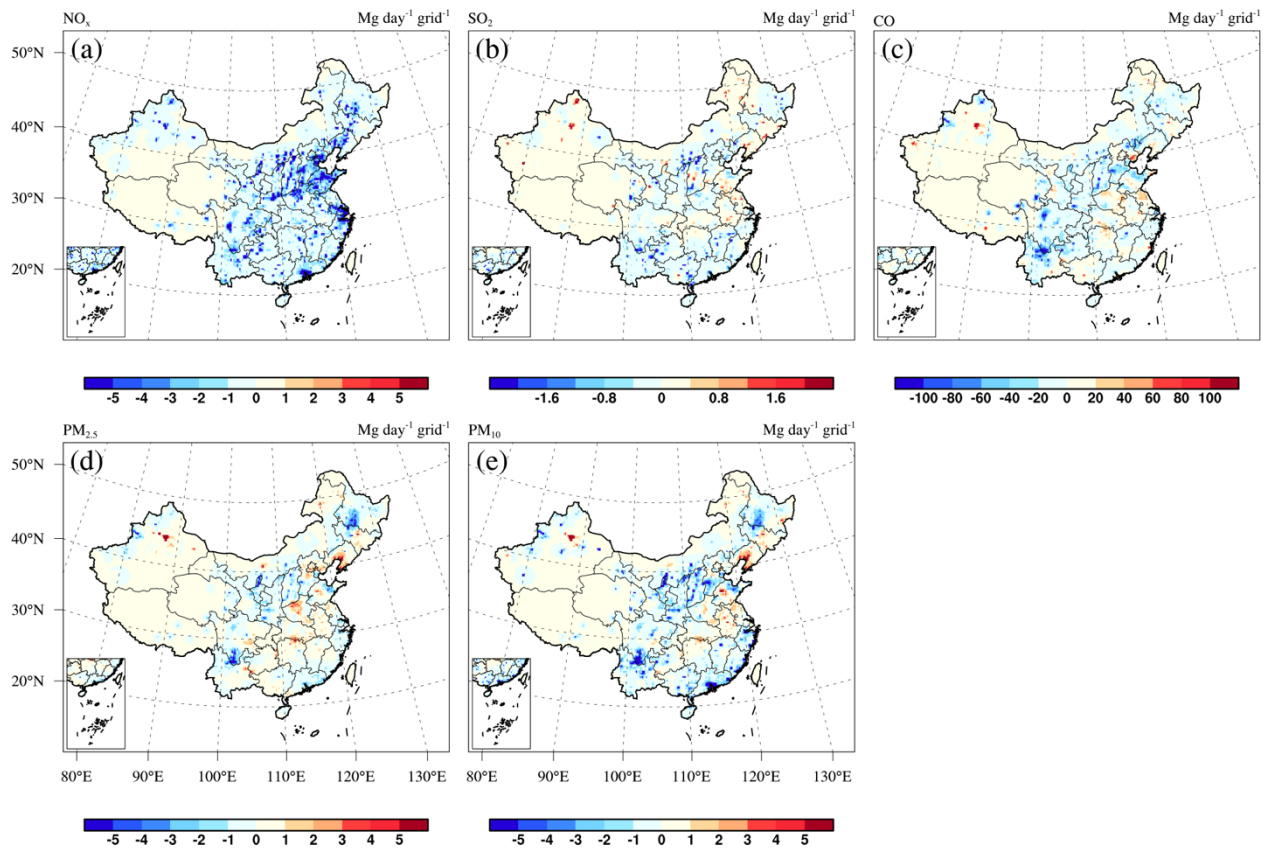
590

591 **Figure 6: The inversion estimated emission changes of (a) NO$_x$, (b) SO$_2$, (c) CO, (d) PM$_{2.5}$ and (e) PM$_{10}$ in China from P1 to P2 period.**

592
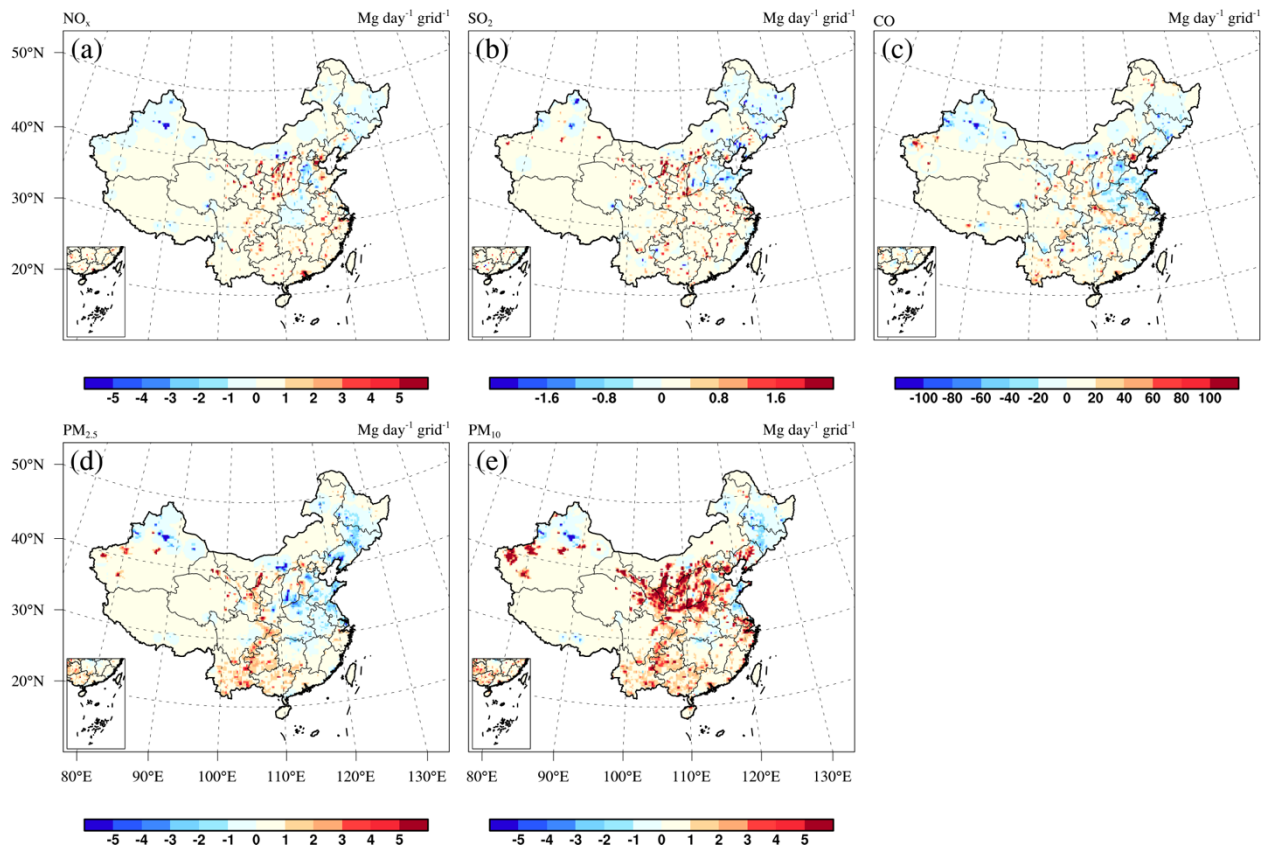
Figure 7: The inversion estimated emission changes of (a) NO$_x$, (b) SO$_2$, (c) CO, (d) PM$_{2.5}$ and (e) PM$_{10}$ in China from P2 to P3 period.

594

595
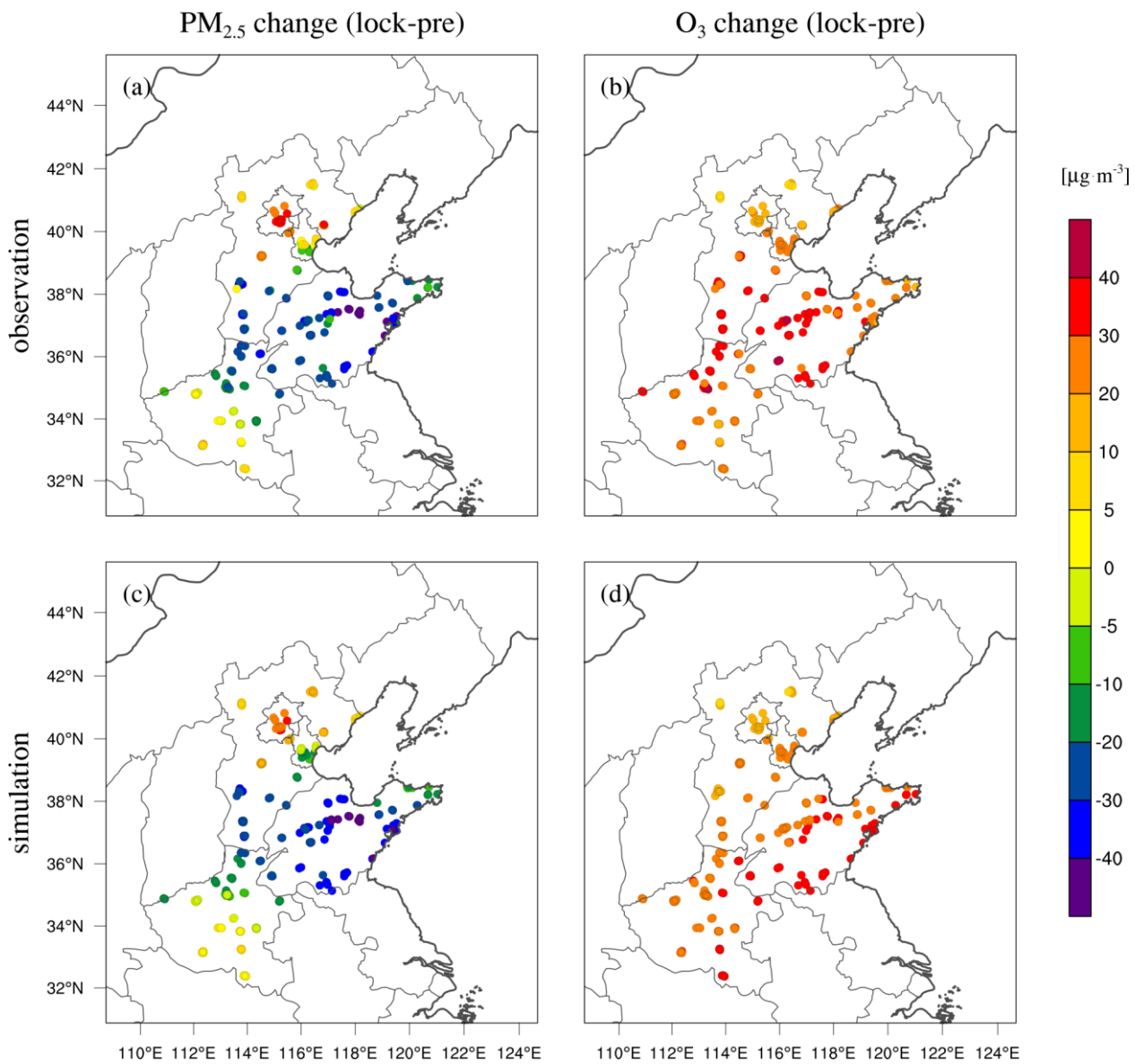
Figure 8: Changes in the observed and simulated concentrations of (a, c) PM₂.₅ and (b, d) O₃ over the NCP region from the pre lockdown period (P1) to the lockdown period (P2).

598
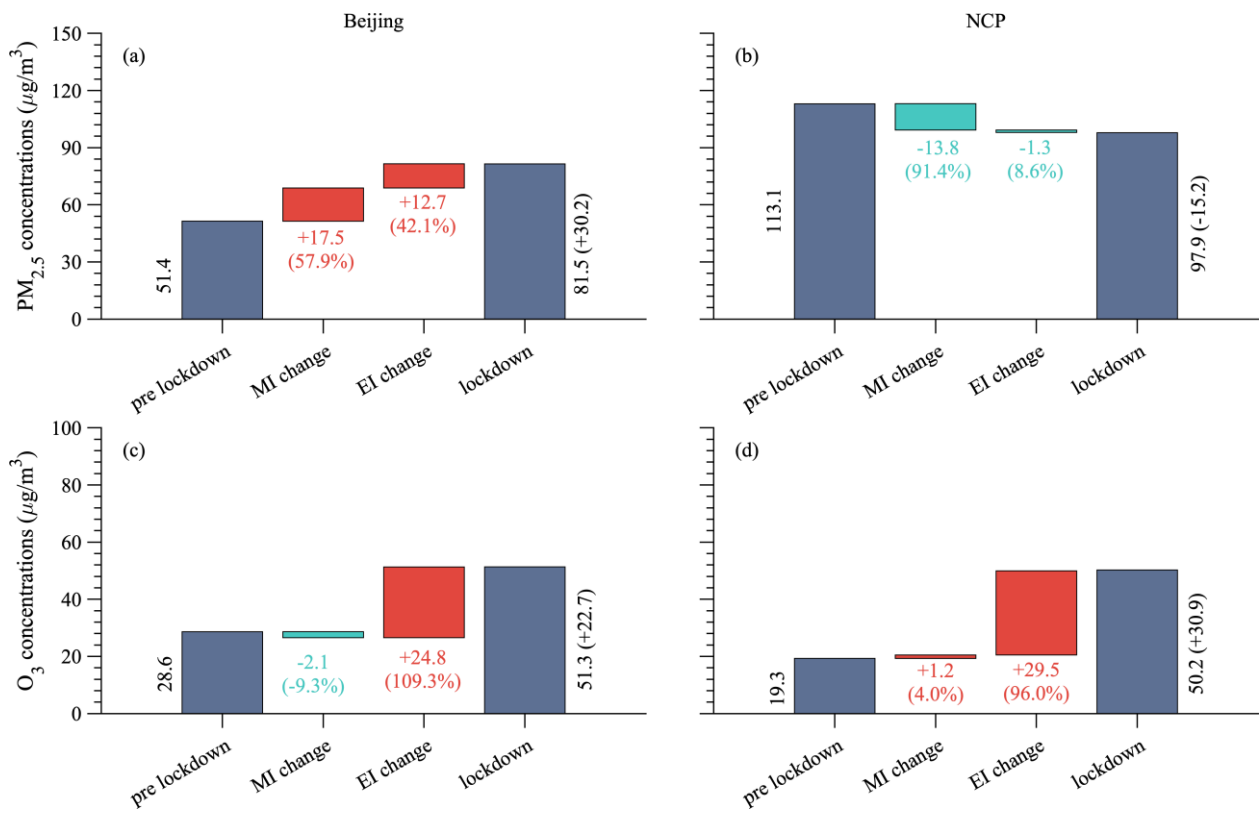
Figure 9: Contributions of the meteorological variations and emission changes to the changes in (a, b) PM$_{2.5}$ and (c, d) O$_3$ concentrations over Beijing and the NCP region from the pre lockdown period (P1) to the lockdown period (P2).
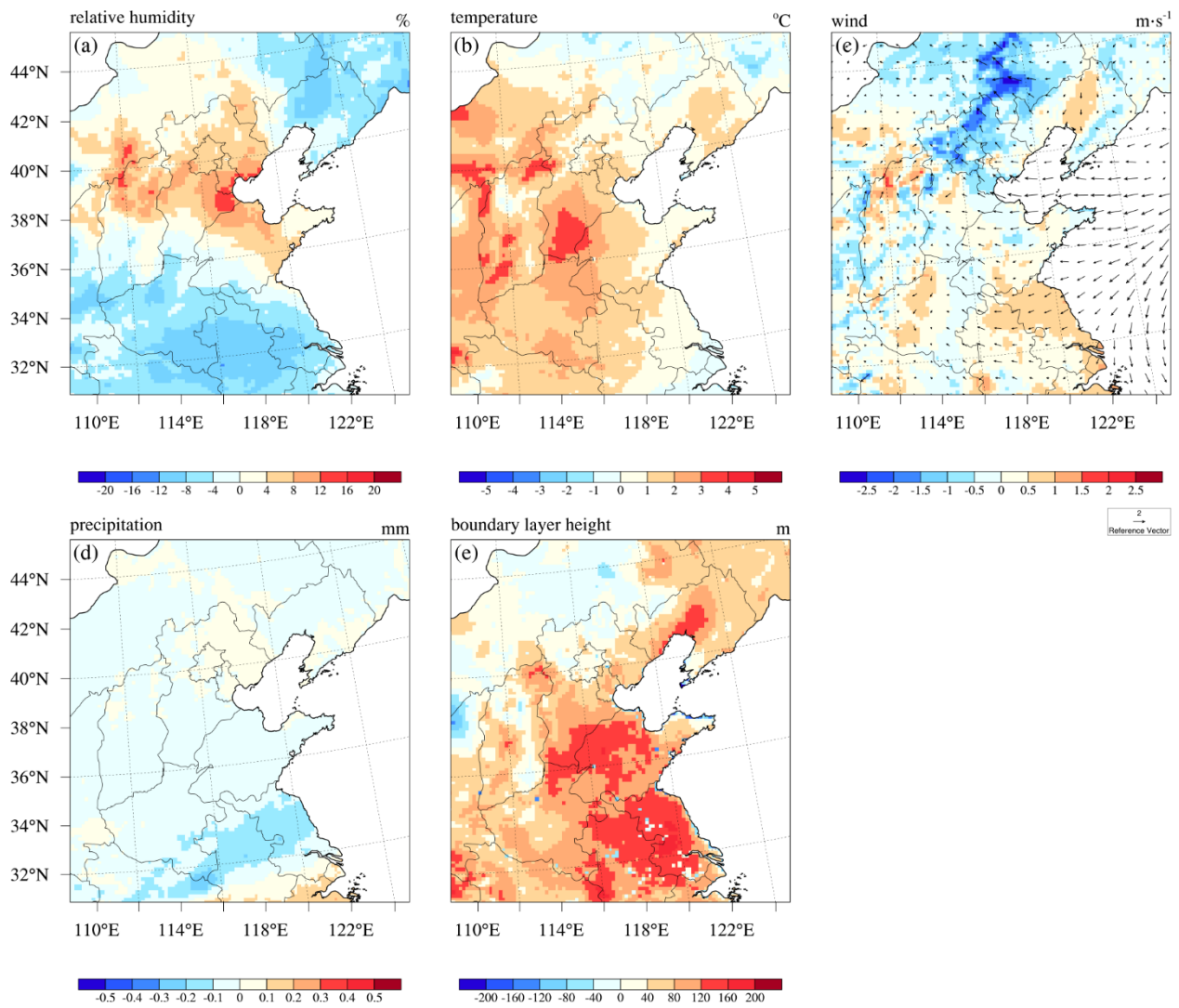
Figure 10: Changes in the (a) relative humidity, (b) temperature, (c) wind speed, (d) precipitation and (e) boundary layer height over the NCP region from P1 to P2 period obtained from WRF simulations.

608
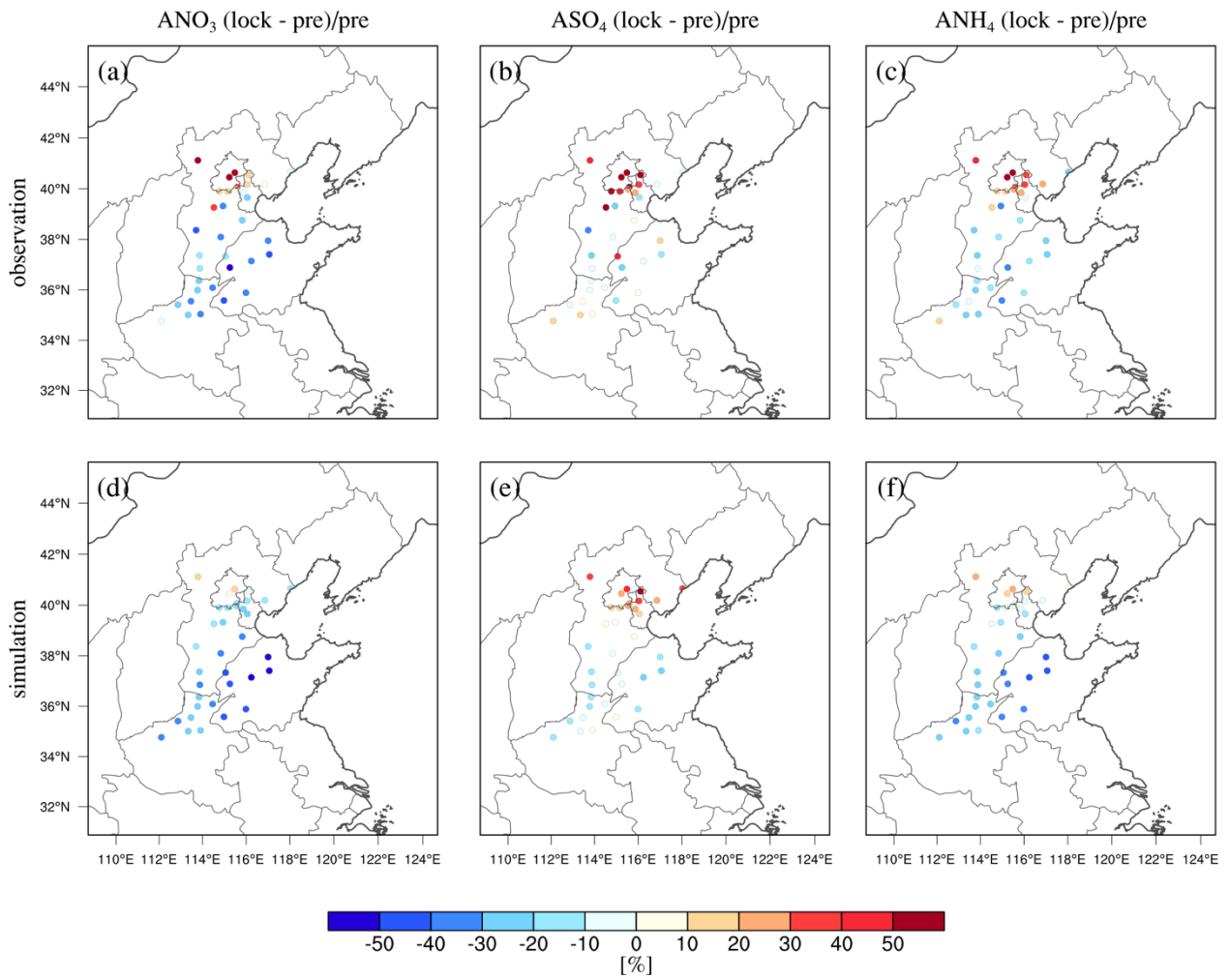
Figure 11: Relative changes in the simulated and observed concentrations of (a) ANO₃, (b) ASO₄, (c) ANH₄ over NCP region from P1 to P2 period.

611

612
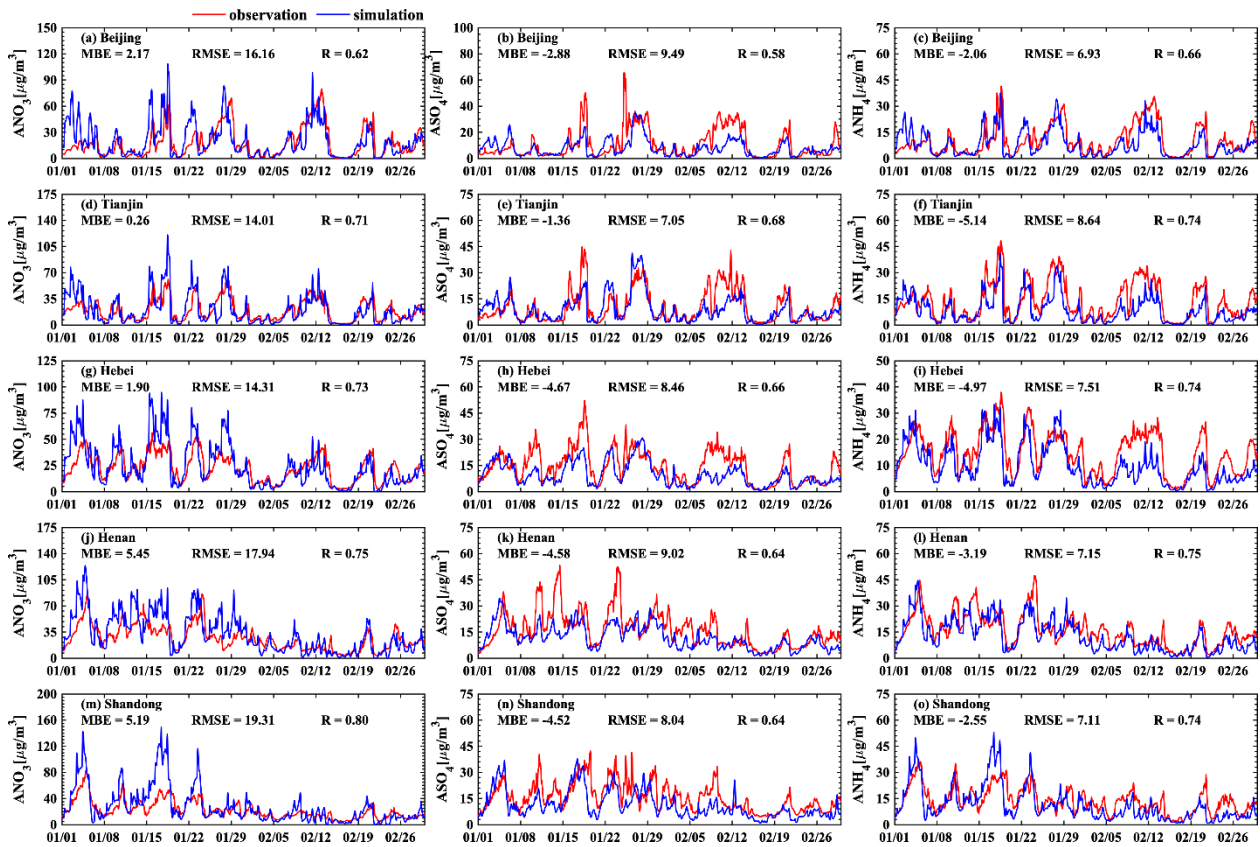
Figure 12: Time series of observed and simulated concentrations of ANO₃, ASO₄ and ANH₄ in (a-c) Beijing, (b-f) Tianjin, (g-i) Heibei, (j-l) Henan and (m-o) Shangdong province from 1st January to 29th February 2020.

613
614

615

616

617
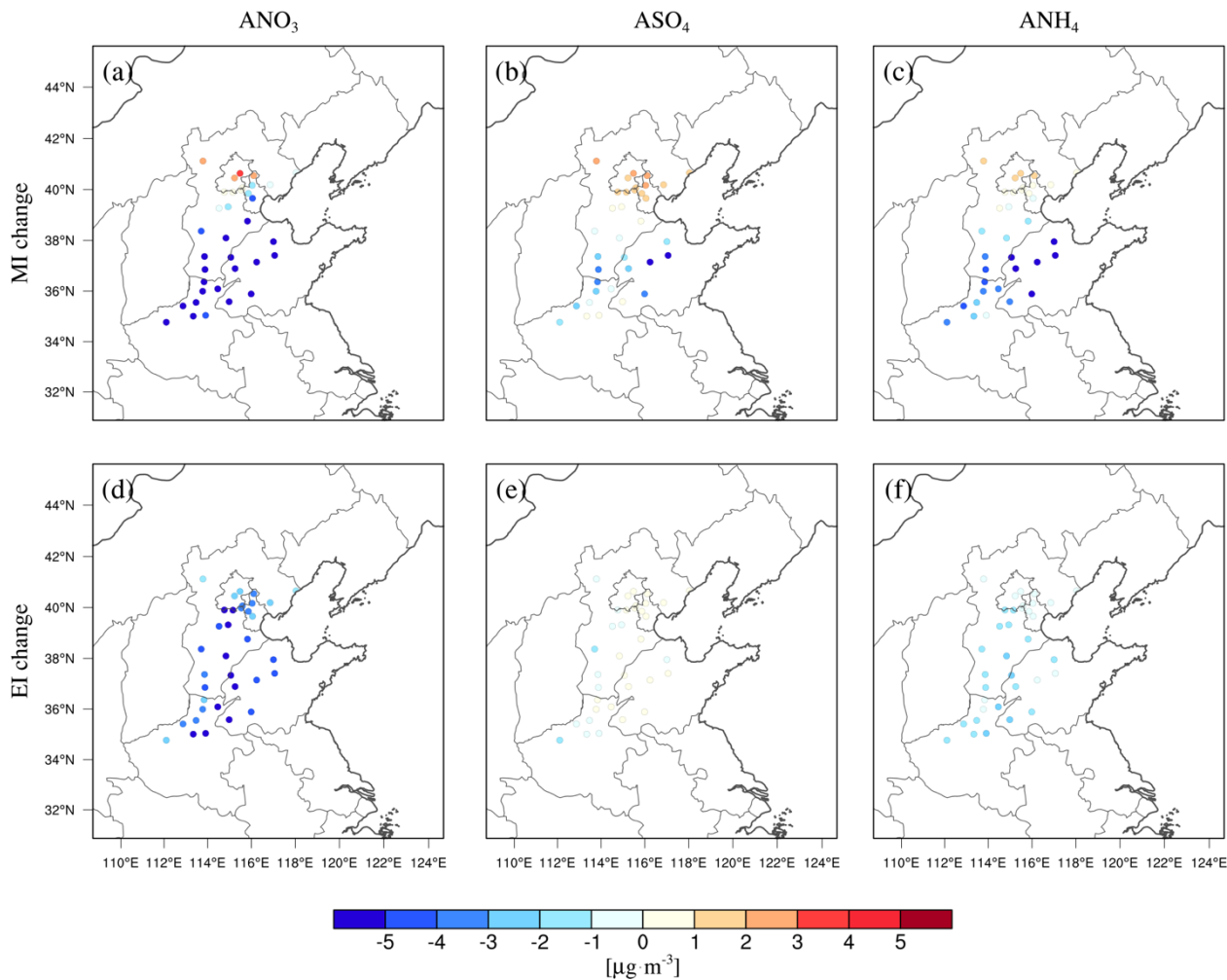
Figure 13: Meteorology-induced (MI) changes in the concentrations of (a) ANO₃, (b) ASO₄ and (c) ANH₄, as well as Emission-induced (EI) changes in the concentrations of (d) ANO₃, (e) ASO₄ and (f) ANH₄.

620

Data availability

The hourly surface observations can be obtained from China National Environmental Monitoring Centre (http://www/cnemc.cn/en); The inversion estimated emissions of multi-air pollutants in China during COVID-19 lockdown period and the NAQPMS simulation results are available from the corresponding authors on request.

Author contributions

X.T., J.Z., and Z.W. conceived and designed the project; H.W., L.K., X.T., and L.W. established the data assimilation system; M.L. Q.W. S.H. W.S. contributed to interpreting the data. L.K. conducted the inversion estimate, drew figures, and wrote the paper with comments provided by J.L., X.P., M.G., P.F., Y.S., H.A. and G.R.C.

Competing interests

The authors declare no competing financial interest.

Acknowledgements

We acknowledge the use of surface air quality observation data from CNEMC. This study has been supported by the National Natural Science Foundation of China (grant nos. 41875164, 91644216, 92044303), the CAS Strategic Priority Research Program (grant no. XDA19040201), the CAS Information Technology Program (grant no. XXH13506-302), and the National Key Scientific and Technological Infrastructure project "Earth System Science Numerical Simulator Facility" (EarthLab).

References

Brasseur, G. P., Hauglustaine, D. A., Walters, S., Rasch, P. J., Muller, J. F., Granier, C., and Tie, X. X.: MOZART, a global chemical transport model for ozone and related chemical tracers 1. Model description, J. Geophys. Res.-Atmos., 103, 28265-28289, https://doi.org/10.1029/98jd02397, 1998.

Cai, H. and Xie, S.: Traffic-related air pollution modeling during the 2008 Beijing Olympic Games: The effects of an odd-even day traffic restriction scheme, Sci. Total Environ., 409, 1935-1948, https://doi.org/10.1016/j.scitotenv.2011.01.025, 2011.

Chen, Z., Hao, X., Zhang, X., and Chen, F.: Have traffic restrictions improved air quality? A shock from COVID-19, J. Clean Prod., 279, 123622, https://doi.org/10.1016/j.jclepro.2020.123622, 2021.

Cheng, C., Barceló, J., Hartnett, A. S., Kubinec, R., and Messerschmidt, L.: COVID-19 Government Response Event Dataset (CoronaNet v.1.0), Nat. Hum. Behav., 4, 756-768, https://doi.org/10.1038/s41562-020-0909-7, 2020.

Chowdhury, S., Dey, S., Tripathi, S. N., Beig, G., Mishra, A. K., and Sharma, S.: "Traffic intervention" policy fails to mitigate air pollution in megacity Delhi, Environ. Sci. Policy, 74, 8-13, https://doi.org/10.1016/j.envsci.2017.04.018, 2017.

Chu, B., Zhang, S., Liu, J., Ma, Q., and He, H.: Significant concurrent decrease in PM2.5 and NO2 concentrations in China during COVID-19 epidemic, J. Environ. Sci., 99, 346-353, https://doi.org/10.1016/j.jes.2020.06.031, 2021.

Chu, K. K., Peng, Z., Liu, Z. Q., Lei, L. L., Kou, X. X., Zhang, Y., Bo, X., and Tian, J.: Evaluating the Impact of Emissions Regulations on the Emissions Reduction During the 2015 China Victory Day Parade With an Ensemble Square Root Filter, J. Geophys. Res.-Atmos., 123, 4122-4134, https://doi.org/10.1002/2017jd027631, 2018.

Cooper, M. J., Martin, R. V., McLinden, C. A., and Brook, J. R.: Inferring ground-level nitrogen dioxide concentrations at fine spatial resolution applied to the TROPOMI satellite instrument, Environ. Res. Lett., 15, 12, https://doi.org/10.1088/1748-9326/aba3a5, 2020.

Crippa, M., Guizzardi, D., Butler, T., Keating, T., Wu, R., Kaminski, J., Kuenen, J., Kurokawa, J., Chatani, S., Morikawa, T., Pouliot, G., Racine, J., Moran, M. D., Klimont, Z., Manseau, P. M., Mashayekhi, R., Henderson, B. H., Smith, S. J., Suchyta, H., Muntean, M., Solazzo, E., Banja, M., Schaaf, E., Pagani, F., Woo, J. H., Kim, J., Monforti-Ferrario, F., Pisoni, E., Zhang, J., Niemi, D., Sassi, M., Ansari, T., and Foley, K.: HTAP_v3 emission mosaic: a global effort to tackle air quality issues by quantifying global anthropogenic air pollutant sources, Earth Syst. Sci. Data Discuss., 2023, 1-34, https://doi.org/10.5194/essd-2022-442, 2023.

Dai, Q., Liu, B., Bi, X., Wu, J., Liang, D., Zhang, Y., Feng, Y., and Hopke, P. K.: Dispersion Normalized PMF Provides Insights into the Significant Changes in Source Contributions to PM2.5 after the COVID-19 Outbreak, Environ. Sci. Technol., 54, 9917-9927, https://doi.org/10.1021/acs.est.0c02776, 2020.

Diamond, M. S. and Wood, R.: Limited Regional Aerosol and Cloud Microphysical Changes Despite Unprecedented Decline in Nitrogen Oxide Pollution During the February 2020 COVID-19 Shutdown in China, Geophys. Res. Lett., 47, e2020GL088913, https://doi.org/10.1029/2020gl088913, 2020.

Dunlea, E. J., Herndon, S. C., Nelson, D. D., Volkamer, R. M., San Martini, F., Sheehy, P. M., Zahniser, M. S., Shorter, J. H., Wormhoudt, J. C., Lamb, B. K., Allwine, E. J., Gaffney, J. S., Marley, N. A., Grutter, M., Marquez, C., Blanco, S., Cardenas, B., Retama, A., Villegas, C. R. R., Kolb, C. E., Molina, L. T., and Molina, M. J.: Evaluation of nitrogen dioxide chemiluminescence monitors in a polluted urban environment, Atmos. Chem. Phys., 7, 2691-2704, https://doi.org/10.5194/acp-7-2691-2007, 2007.

Evensen, G.: Sequential data assimilation with a nonlinear quasi-geostrophic model using Monte Carlo methods to forecast error statistics, J. Geophys. Res.-Oceans, 99, 10143-10162, https://doi.org/10.1029/94JC00572, 1994.

Fan, C., Li, Y., Guang, J., Li, Z. Q., Elnashar, A., Allam, M., and de Leeuw, G.: The Impact of the Control Measures during the COVID-19 Outbreak on Air Pollution in China, Remote Sens., 12, 23, https://doi.org/10.3390/rs12101613, 2020.

Fan, H., Zhao, C., Yang, Y., and Yang, X.: Spatio-Temporal Variations of the PM2.5/PM10 Ratios and Its Application to Air Pollution Type Classification in China, Front. Environ. Sci., 9, https://doi.org/10.3389/fenvs.2021.692440, 2021.

Feng, S., Jiang, F., Wang, H., Wang, H., Ju, W., Shen, Y., Zheng, Y., Wu, Z., and Ding, A.: NOx Emission Changes Over China During the COVID-19 Epidemic Inferred From Surface NO2 Observations, Geophys. Res. Lett., 47, e2020GL090080, 10.1029/2020gl090080, 2020.

Forster, P. M., Forster, H. I., Evans, M. J., Gidden, M. J., Jones, C. D., Keller, C. A., Lamboll, R. D., Le Quere, C., Rogelj, J., Rosen, D., Schleussner, C. F., Richardson, T. B., Smith, C. J., and Turnock, S. T.: Current and future global climate impacts resulting from COVID-19, Nat. Clim. Chang., 10, 913-+, https://doi.org/10.1038/s41558-020-0883-0, 2020.

Granier, C., Lamarque, J., Mieville, A., Muller, J., Olivier, J., Orlando, J., Peters, J., Petron, G., Tyndall, G., and Wallens, S.: POET, a database of surface emissions of ozone precursors, 2005.

Hammer, M. S., van Donkelaar, A., Martin, R. V., McDuffie, E. E., Lyapustin, A., Sayer, A. M., Hsu, N. C., Levy, R. C., Garay, M. J., Kalashnikova, O. V., and Kahn, R. A.: Effects of COVID-19 lockdowns on fine particulate matter concentrations, Sci. Adv., 7, https://doi.org/10.1126/sciadv.abg7670, 2021.

Han, X. L. and Naeher, L. P.: A review of traffic-related air pollution exposure assessment studies in the developing world, Environ. Int., 32, 106-120, https://doi.org/10.1016/j.envint.2005.05.020, 2006.

Hauglustaine, D. A., Brasseur, G. P., Walters, S., Rasch, P. J., Muller, J. F., Emmons, L. K., and Carroll, C. A.: MOZART, a global chemical transport model for ozone and related chemical tracers 2. Model results and evaluation, J. Geophys. Res.-Atmos., 103, 28291-28335, https://doi.org/10.1029/98jd02398, 1998.

He, G. J., Pan, Y. H., and Tanaka, T.: The short-term impacts of COVID-19 lockdown on urban air pollution in China, Nat. Sustain., 3, 9, https://doi.org/10.1038/s41893-020-0581-y, 2020.

693   He, T. L., Jones, D. B. A., Miyazaki, K., Bowman, K. W., Jiang, Z., Chen, X., Li, R., Zhang, Y., and Li, K.: Inverse modelling of Chinese
694   NOx emissions using deep learning: integrating in situ observations with a satellite-based chemical reanalysis, Atmos. Chem. Phys., 22,
695   14059-14074, https://doi.org/10.5194/acp-22-14059-2022, 2022.

696   Hu, Y., Zang, Z., Ma, X., Li, Y., Liang, Y., You, W., Pan, X., and Li, Z.: Four-dimensional variational assimilation for SO2 emission and its
697   application around the COVID-19 lockdown in the spring 2020 over China, Atmos. Chem. Phys., 22, 13183-13200,
698   https://doi.org/10.5194/acp-22-13183-2022, 2022.

699   Huang, X., Ding, A., Gao, J., Zheng, B., Zhou, D., Qi, X., Tang, R., Wang, J., Ren, C., Nie, W., Chi, X., Xu, Z., Chen, L., Li, Y., Che, F.,
700   Pang, N., Wang, H., Tong, D., Qin, W., Cheng, W., Liu, W., Fu, Q., Liu, B., Chai, F., Davis, S. J., Zhang, Q., and He, K.: Enhanced
701   secondary pollution offset reduction of primary emissions during COVID-19 lockdown in China, Natl. Sci. Rev., 8,
702   https://doi.org/10.1093/nsr/nwaa137, 2021.

703   Janssens-Maenhout, G., Crippa, M., Guizzardi, D., Dentener, F., Muntean, M., Pouliot, G., Keating, T., Zhang, Q., Kurokawa, J., Wankmuller,
704   R., van der Gon, H. D., Kuenen, J. J. P., Klimont, Z., Frost, G., Darras, S., Koffi, B., and Li, M.: HTAP_v2.2: a mosaic of regional and
705   global emission grid maps for 2008 and 2010 to study hemispheric transport of air pollution, Atmos. Chem. Phys., 15, 11411-11432,
706   https://doi.org/10.5194/acp-15-11411-2015, 2015.

707   Kaiser, J. W., Heil, A., Andreae, M. O., Benedetti, A., Chubarova, N., Jones, L., Morcrette, J. J., Razinger, M., Schultz, M. G., Suttie, M.,
708   and van der Werf, G. R.: Biomass burning emissions estimated with a global fire assimilation system based on observed fire radiative
709   power, Biogeosciences, 9, 527-554, https://doi.org/10.5194/bg-9-527-2012, 2012.

710   Kong, L., Tang, X., Zhu, J., Wang, Z., Pan, Y., Wu, H., Wu, L., Wu, Q., He, Y., Tian, S., Xie, Y., Liu, Z., Sui, W., Han, L., and Carmichael,
711   G.: Improved Inversion of Monthly Ammonia Emissions in China Based on the Chinese Ammonia Monitoring Network and Ensemble
712   Kalman Filter, Environ. Sci. Technol., 53, 12529-12538, https://doi.org/10.1021/acs.est.9b02701, 2019.

713   Kong, L., Tang, X., Zhu, J., Wang, Z., Li, J., Wu, H., Wu, Q., Chen, H., Zhu, L., Wang, W., Liu, B., Wang, Q., Chen, D., Pan, Y., Song, T.,
714   Li, F., Zheng, H., Jia, G., Lu, M., Wu, L., and Carmichael, G. R.: A 6-year-long (2013–2018) high-resolution air quality reanalysis dataset
715   in China based on the assimilation of surface observations from CNEMC, Earth Syst. Sci. Data, 13, 529-570, https://doi.org/10.5194/essd-
716   13-529-2021, 2021.

717   Lamsal, L. N., Martin, R. V., van Donkelaar, A., Steinbacher, M., Celarier, E. A., Bucsela, E., Dunlea, E. J., and Pinto, J. P.: Ground-level
718   nitrogen dioxide concentrations inferred from the satellite-borne Ozone Monitoring Instrument, J. Geophys. Res.-Atmos., 113,
719   https://doi.org/10.1029/2007JD009235, 2008.

720   Le, T. H., Wang, Y., Liu, L., Yang, J. N., Yung, Y. L., Li, G. H., and Seinfeld, J. H.: Unexpected air pollution with marked emission reductions
721   during the COVID-19 outbreak in China, Science, 369, 702-+, https://doi.org/10.1126/science.abb7431, 2020.

722   Levelt, P. F., Stein Zweers, D. C., Aben, I., Bauwens, M., Borsdorff, T., De Smedt, I., Eskes, H. J., Lerot, C., Loyola, D. G., Romahn, F.,
723   Stavrakou, T., Theys, N., Van Roozendael, M., Veefkind, J. P., and Verhoelst, T.: Air quality impacts of COVID-19 lockdown measures
724   detected from space using high spatial resolution observations of multiple trace gases from Sentinel-5P/TROPOMI, Atmos. Chem. Phys.,
725   22, https://doi.org/10319-10351, 10.5194/acp-22-10319-2022, 2022.

726   Li, B., Fan, J., Han, L., Sun, G., Zhang, D., and Zhang, P.: An Industrial Heat Source Extraction Method: BP Neural Network Using
727   Temperature Feature Template (in Chinese with English abstract), Journal of Geo-Information Science, 24, 533-545, 2022.

728   Li, F., Tang, X., Wang, Z., Zhu, L., Wang, X., Wu, H., Lu, M., Li, J., and Zhu, J.: Estimation of Representative Errors of Surface Observations
729   of Air Pollutant Concentrations Based on High-Density Observation Network over Beijing-Tianjin-Hebei Region, Chinese Journal of
730   Atmospheric Sciences, 43, 277-284, 2019.

731 Li, L., Li, Q., Huang, L., Wang, Q., Zhu, A., Xu, J., Liu, Z., Li, H., Shi, L., Li, R., Azari, M., Wang, Y., Zhang, X., Liu, Z., Zhu, Y., Zhang,
732   K., Xue, S., Ooi, M. C. G., Zhang, D., and Chan, A.: Air quality changes during the COVID-19 lockdown over the Yangtze River Delta
733   Region: An insight into the impact of human activity pattern changes on air pollution variation, Sci. Total Environ., 732, 139282,
734   https://doi.org/10.1016/j.scitotenv.2020.139282, 2020.

735 Li, M., Wang, T., Xie, M., Li, S., Zhuang, B., Fu, Q., Zhao, M., Wu, H., Liu, J., Saikawa, E., and Liao, K.: Drivers for the poor air quality
736   conditions   in   North   China   Plain   during   the   COVID-19   outbreak,   Atmos.   Environ.,   246,   118103,
737   https://doi.org/10.1016/j.atmosenv.2020.118103, 2021.

738 Li, M., Liu, H., Geng, G. N., Hong, C. P., Liu, F., Song, Y., Tong, D., Zheng, B., Cui, H. Y., Man, H. Y., Zhang, Q., and He, K. B.:
739   Anthropogenic emission inventories in China: a review, Natl. Sci. Rev., 4, 834-866, https://doi.org/10.1093/nsr/nwx150, 2017a.

740 Li, M., Zhang, Q., Kurokawa, J. I., Woo, J. H., He, K., Lu, Z., Ohara, T., Song, Y., Streets, D. G., Carmichael, G. R., Cheng, Y., Hong, C.,
741   Huo, H., Jiang, X., Kang, S., Liu, F., Su, H., and Zheng, B.: MIX: a mosaic Asian anthropogenic emission inventory under the international
742   collaboration framework of the MICS-Asia and HTAP, Atmos. Chem. Phys., 17, 935-963, https://doi.org/10.5194/acp-17-935-2017, 2017b.

743 Li, M., Zhang, Q., Zheng, B., Tong, D., Lei, Y., Liu, F., Hong, C. P., Kang, S. C., Yan, L., Zhang, Y. X., Bo, Y., Su, H., Cheng, Y. F., and
744   He, K. B.: Persistent growth of anthropogenic non-methane volatile organic compound (NMVOC) emissions in China during 1990-2017:
745   drivers, speciation and ozone formation potential, Atmos. Chem. Phys., 19, 8897-8913, https://doi.org/10.5194/acp-19-8897-2019, 2019.

746 Li, X., Zhang, Q., Zhang, Y., Zhang, L., Wang, Y. X., Zhang, Q. Q., Li, M., Zheng, Y. X., Geng, G. N., Wallington, T. J., Han, W. J., Shen,
747   W., and He, K. B.: Attribution of PM2.5 exposure in Beijing-Tianjin-Hebei region to emissions: implication to control strategies, Sci.
748   Bull., 62, 957-964, https://doi.org/10.1016/j.scib.2017.06.005, 2017c.

749 Ma, C. Q., Wang, T. J., Mizzi, A. P., Anderson, J. L., Zhuang, B. L., Xie, M., and Wu, R. S.: Multiconstituent Data Assimilation With WRF-
750   Chem/DART: Potential for Adjusting Anthropogenic Emissions and Improving Air Quality Forecasts Over Eastern China, J. Geophys.
751   Res.-Atmos., 124, 7393-7412, https://doi.org/10.1029/2019jd030421, 2019.

752 Ma, T., Duan, F. K., Ma, Y. L., Zhang, Q. Q., Xu, Y. Z., Li, W. G., Zhu, L. D., and He, K. B.: Unbalanced emission reductions and adverse
753   meteorological conditions facilitate the formation of secondary pollutants during the COVID-19 lockdown in Beijing, Sci. Total Environ.,
754   838, 8, https://doi.org/10.1016/j.scitotenv.2022.155970, 2022.

755 Miyazaki, K., Eskes, H. J., Sudo, K., Takigawa, M., van Weele, M., and Boersma, K. F.: Simultaneous assimilation of satellite NO2, O-3,
756   CO, and HNO3 data for the analysis of tropospheric chemical composition and emissions, Atmos. Chem. Phys., 12, 9545-9579,
757   https://doi.org/10.5194/acp-12-9545-2012, 2012.

758 Okuda, T., Matsuura, S., Yamaguchi, D., Umemura, T., Hanada, E., Orihara, H., Tanaka, S., He, K., Ma, Y., Cheng, Y., and Liang, L.: The
759   impact of the pollution control measures for the 2008 Beijing Olympic Games on the chemical composition of aerosols, Atmos. Environ.,
760   45, 2789-2794, https://doi.org/10.1016/j.atmosenv.2011.01.053, 2011.

761 Peng, Z., Lei, L. L., Liu, Z. Q., Su, J. N., Ding, A. J., Ban, J. M., Chen, D., Kou, X. X., and Chu, K. K.: The impact of multi-species surface
762   chemical observation assimilation on air quality forecasts in China, Atmos. Chem. Phys., 18, 18, https://doi.org/10.5194/acp-18-17387-
763   2018, 2018.

764 Price, C., Penner, J., and Prather, M.: NOx from lightning .1. Global distribution based on lightning physics, J. Geophys. Res.-Atmos., 102,
765   5929-5941, https://doi.org/10.1029/96jd03504, 1997.

766 Randerson, J. T., Van Der Werf, G. R., Giglio, L., Collatz, G. J., and Kasibhatla, P. S.: Global Fire Emissions Database, Version 4.1 (GFEDv4),
767   10.3334/ornldaac/1293, 2017.

768   Sakov, P. and Oke, P. R.: A deterministic formulation of the ensemble Kalman filter: an alternative to ensemble square root filters, Tellus

769   Ser. A-Dyn. Meteorol. Oceanol., 60, 361-371, https://doi.org/10.1111/j.1600-0870.2007.00299.x, 2008.

770   Skachko, S., Errera, Q., Ménard, R., Christophe, Y., and Chabrillat, S.: Comparison of the ensemble Kalman filter and 4D-Var assimilation

771   methods using a stratospheric tracer transport model, Geosci. Model Dev., 7, 1451-1465, https://doi.org/10.5194/gmd-7-1451-2014, 2014.

772   Shi, X. and Brasseur, G. P.: The Response in Air Quality to the Reduction of Chinese Economic Activities During the COVID-19 Outbreak,

773   Geophys. Res. Lett., 47, e2020GL088070, https://doi.org/10.1029/2020gl088070, 2020.

774   Shi, Z., Song, C., Liu, B., Lu, G., Xu, J., Van Vu, T., Elliott, R. J. R., Li, W., Bloss, W. J., and Harrison, R. M.: Abrupt but smaller than

775   expected   changes   in   surface   air   quality   attributable   to   COVID-19   lockdowns,   Sci.   Adv.,   7,   eabd6696,

776   https://doi.org/10.1126/sciadv.abd6696, 2021.

777   Sindelarova, K., Granier, C., Bouarar, I., Guenther, A., Tilmes, S., Stavrakou, T., Muller, J. F., Kuhn, U., Stefani, P., and Knorr, W.: Global

778   data set of biogenic VOC emissions calculated by the MEGAN model over the last 30 years, Atmos. Chem. Phys., 14, 9317-9341,

779   https://doi.org/10.5194/acp-14-9317-2014, 2014.

780   Skamarock, W. C.: A description of the advanced research WRF version 3, Ncar Technical, 113, 7-25, 2008.

781   Song, Y. S., Lin, C. Q., Li, Y., Lau, A. K. H., Fung, J. C. H., Lu, X. C., Guo, C., Ma, J., and Lao, X. Q.: An improved decomposition method

782   to differentiate meteorological and anthropogenic effects on air pollution: A national study in China during the COVID-19 lockdown

783   period, Atmos. Environ., 250, 9, https://doi.org/10.1016/j.atmosenv.2021.118270, 2021.

784   Streets, D. G., Bond, T. C., Carmichael, G. R., Fernandes, S. D., Fu, Q., He, D., Klimont, Z., Nelson, S. M., Tsai, N. Y., Wang, M. Q., Woo,

785   J. H., and Yarber, K. F.: An inventory of gaseous and primary aerosol emissions in Asia in the year 2000, J. Geophys. Res.-Atmos., 108,

786   23, https://doi.org/10.1029/2002JD003093, 2003.

787   Streets, D. G., Canty, T., Carmichael, G. R., de Foy, B., Dickerson, R. R., Duncan, B. N., Edwards, D. P., Haynes, J. A., Henze, D. K.,

788   Houyoux, M. R., Jacob, D. J., Krotkov, N. A., Lamsal, L. N., Liu, Y., Lu, Z., Martin, R. V., Pfister, G. G., Pinder, R. W., Salawitch, R. J.,

789   and Wecht, K. J.: Emissions estimation from satellite retrievals: A review of current capability, Atmos. Environ., 77, 1011-1042,

790   https://doi.org/10.1016/j.atmosenv.2013.05.051, 2013.

791   Sulaymon, I. D., Zhang, Y., Hopke, P. K., Hu, J., Zhang, Y., Li, L., Mei, X., Gong, K., Shi, Z., Zhao, B., and Zhao, F.: Persistent high PM2.5

792   pollution driven by unfavorable meteorological conditions during the COVID-19 lockdown period in the Beijing-Tianjin-Hebei region,

793   China, Environ. Res., 198, 111186, https://doi.org/10.1016/j.envres.2021.111186, 2021.

794   Tandeo, P., Ailliot, P., Bocquet, M., Carrassi, A., Miyoshi, T., Pulido, M., and Zhen, Y. C.: A Review of Innovation-Based Methods to Jointly

795   Estimate Model and Observation Error Covariance Matrices in Ensemble Data Assimilation, Mon. Weather Rev., 148, 3973-3994,

796   https://doi.org/10.1175/mwr-d-19-0240.1, 2020.

797   Tang, G., Zhu, X., Hu, B., Xin, J., Wang, L., Münkel, C., Mao, G., and Wang, Y.: Impact of emission controls on air quality in Beijing during

798   APEC 2014: lidar ceilometer observations, Atmos. Chem. Phys., 15, 12667-12680, https://doi.org/10.5194/acp-15-12667-2015, 2015.

799   Tang, X., Zhu, J., Wang, Z. F., and Gbaguidi, A.: Improvement of ozone forecast over Beijing based on ensemble Kalman filter with

800   simultaneous adjustment of initial conditions and emissions, Atmos. Chem. Phys., 11, 12901-12916, 10.5194/acp-11-12901-2011, 2011.

801   Tang, X., Zhu, J., Wang, Z. F., Wang, M., Gbaguidi, A., Li, J., Shao, M., Tang, G. Q., and Ji, D. S.: Inversion of CO emissions over Beijing

802   and its surrounding areas with ensemble Kalman filter, Atmos. Environ., 81, 676-686, https://doi.org/10.1016/j.atmosenv.2013.08.051,

803   2013.

804 van der Werf, G. R., Randerson, J. T., Giglio, L., Collatz, G. J., Mu, M., Kasibhatla, P. S., Morton, D. C., DeFries, R. S., Jin, Y., and van
805   Leeuwen, T. T.: Global fire emissions and the contribution of deforestation, savanna, forest, agricultural, and peat fires (1997–2009),
806   Atmos. Chem. Phys., 10, 11707-11735, https://doi.org/10.5194/acp-10-11707-2010, 2010.

807 Wang, P., Chen, K., Zhu, S., Wang, P., and Zhang, H.: Severe air pollution events not avoided by reduced anthropogenic activities during
808   COVID-19 outbreak, Resour. Conserv. Recycl., 158, 104814, https://doi.org/10.1016/j.resconrec.2020.104814, 2020.

809 Wang, S., Gao, J., Zhang, Y., Zhang, J., Cha, F., Wang, T., Ren, C., and Wang, W.: Impact of emission control on regional air quality: An
810   observational study of air pollutants before, during and after the Beijing Olympic Games, J. Environ. Sci., 26, 175-180,
811   https://doi.org/10.1016/S1001-0742(13)60395-2, 2014.

812 Wang, Y. Q., Zhang, X. Y., Sun, J. Y., Zhang, X. C., Che, H. Z., and Li, Y.: Spatial and temporal variations of the concentrations of PM_{10},
813   $PM_{2.5}$ and PM_1 in China, Atmos. Chem. Phys., 15, 13585-13598, https://doi.org/10.5194/acp-15-13585-2015, 2015.

814 Wang, Z., Uno, I., Yumimoto, K., Itahashi, S., Chen, X., Yang, W., and Wang, Z.: Impacts of COVID-19 lockdown, Spring Festival and
815   meteorology on the NO2 variations in early 2020 over China based on in-situ observations, satellite retrievals and model simulations,
816   Atmos. Environ., 244, 117972, https://doi.org/10.1016/j.atmosenv.2020.117972, 2021.

817 Wu, H., Tang, X., Wang, Z., Wu, L., Li, J., Wang, W., Yang, W., and Zhu, J.: High-spatiotemporal-resolution inverse estimation of CO and
818   NOx emission reductions during emission control periods with a modified ensemble Kalman filter, Atmos. Environ., 236, 117631,
819   https://doi.org/10.1016/j.atmosenv.2020.117631, 2020.

820 Wu, H. J., Tang, X., Wang, Z. F., Wu, L., Lu, M. M., Wei, L. F., and Zhu, J.: Probabilistic Automatic Outlier Detection for Surface Air
821   Quality Measurements from the China National Environmental Monitoring Network, Adv. Atmos. Sci., 35, 1522-1532,
822   https://doi.org/10.1007/s00376-018-8067-9, 2018.

823 Xing, J., Li, S. W., Jiang, Y. Q., Wang, S. X., Ding, D., Dong, Z. X., Zhu, Y., and Hao, J. M.: Quantifying the emission changes and associated
824   air quality impacts during the COVID-19 pandemic on the North China Plain: a response modeling study, Atmos. Chem. Phys., 20, 14347-
825   14359, https://doi.org/10.5194/acp-20-14347-2020, 2020.

826 Yan, C., Shen, Y. C., Stolzenburg, D., Dada, L., Qi, X. M., Hakala, S., Sundstrom, A. M., Guo, Y. S., Lipponen, A., Kokkonen, T. V.,
827   Kontkanen, J., Cai, R. L., Cai, J., Chan, T., Chen, L. D., Chu, B. W., Deng, C. J., Du, W., Fan, X. L., He, X. C., Kangasluoma, J., Kujansuu,
828   J., Kurppa, M., Li, C., Li, Y. R., Lin, Z. H., Liu, Y. L., Liu, Y. L., Lu, Y. Q., Nie, W., Pulliainen, J., Qiao, X. H., Wang, Y. H., Wen, Y.
829   F., Wu, Y., Yang, G., Yao, L., Yin, R. J., Zhang, G., Zhang, S. J., Zheng, F. X., Zhou, Y., Arola, A., Tamminen, J., Paasonen, P., Sun, Y.
830   L., Wang, L., Donahue, N. M., Liu, Y. C., Bianchi, F., Daellenbach, K. R., Worsnop, D. R., Kerminen, V. M., Petaja, T., Ding, A. J., Jiang,
831   J. K., and Kulmala, M.: The effect of COVID-19 restrictions on atmospheric new particle formation in Beijing, Atmos. Chem. Phys., 22,
832   12207-12220, https://doi.org/10.5194/acp-22-12207-2022, 2022.

833 Yan, X. Y., Akimoto, H., and Ohara, T.: Estimation of nitrous oxide, nitric oxide and ammonia emissions from croplands in East, Southeast
834   and South Asia, Glob. Change Biol., 9, 1080-1096, https://doi.org/10.1046/j.1365-2486.2003.00649.x, 2003.

835 Zhang, L., Shao, J., Lu, X., Zhao, Y., Hu, Y., Henze, D. K., Liao, H., Gong, S., and Zhang, Q.: Sources and Processes Affecting Fine
836   Particulate Matter Pollution over North China: An Adjoint Analysis of the Beijing APEC Period, Environ. Sci. Technol., 50, 8731-8740,
837   https://doi.org/10.1021/acs.est.6b03010, 2016.

838 Zhang, Q., Pan, Y., He, Y., Walters, W. W., Ni, Q., Liu, X., Xu, G., Shao, J., and Jiang, C.: Substantial nitrogen oxides emission reduction
839   from China due to COVID-19 and its impact on surface ozone and aerosol pollution, Sci. Total Environ., 753, 142238,
840   https://doi.org/10.1016/j.scitotenv.2020.142238, 2021.

841 Zhang, R. X., Zhang, Y. Z., Lin, H. P., Feng, X., Fu, T. M., and Wang, Y. H.: NOx Emission Reduction and Recovery during COVID-19 in
842   East China, Atmosphere, 11, 15, https://doi.org/10.3390/atmos11040433, 2020.

843 Zhang, W., Guo, J. H., Sun, Y. L., Yuan, H., Zhuang, G. S., Zhuang, Y. H., and Hao, Z. P.: Source apportionment for,urban PM10 and PM2.5
844   in the Beijing area, Chin. Sci. Bull., 52, 608-615, https://doi.org/10.1007/s11434-007-0076-5, 2007.

845 Zhao, X., Wang, G., Wang, S., Zhao, N., Zhang, M., and Yue, W.: Impacts of COVID-19 on air quality in mid-eastern China: An insight into
846   meteorology and emissions, Atmos. Environ., 266, 118750, https://doi.org/10.1016/j.atmosenv.2021.118750, 2021.

847 Zhao, Y. B., Zhang, K., Xu, X. T., Shen, H. Z., Zhu, X., Zhang, Y. X., Hu, Y. T., and Shen, G. F.: Substantial Changes in Nitrogen Dioxide
848   and Ozone after Excluding Meteorological Impacts during the COVID-19 Outbreak in Mainland China, Environ. Sci. Technol. Lett., 7,
849   402-408, https://doi.org/10.1021/acs.estlett.0c00304, 2020.

850 Zheng, B., Zhang, Q., Geng, G., Chen, C., Shi, Q., Cui, M., Lei, Y., and He, K.: Changes in China's anthropogenic emissions and air quality
851   during the COVID-19 pandemic in 2020, Earth Syst. Sci. Data, 13, 2895-2907, https://doi.org/10.5194/essd-13-2895-2021, 2021.

852 Zheng, B., Tong, D., Li, M., Liu, F., Hong, C. P., Geng, G. N., Li, H. Y., Li, X., Peng, L. Q., Qi, J., Yan, L., Zhang, Y. X., Zhao, H. Y.,
853   Zheng, Y. X., He, K. B., and Zhang, Q.: Trends in China's anthropogenic emissions since 2010 as the consequence of clean air actions,
854   Atmos. Chem. Phys., 18, 14095-14111, https://doi.org/10.5194/acp-18-14095-2018, 2018.

855 Zuo, P. J., Zong, Z., Zheng, B., Bi, J. Z., Zhang, Q. H., Li, W., Zhang, J. W., Yang, X. Z., Chen, Z. G., Yang, H., Lu, D. W., Zhang, Q. H.,
856   Liu, Q., and Jiang, G. B.: New Insights into Unexpected Severe PM2.5 Pollution during the SARS and COVID-19 Pandemic Periods in
857   Beijing, Environ. Sci. Technol., 56, 155-164, https://doi.org/10.1021/acs.est.1c05383, 2022.